of infarct size, pretreatment with 4-HNE significantly attenuated the increase in 4-HNE adduct proteins during reperfusion injury (Supplemental Fig. 4).

3.7. 4-HNE treatment has no effect on the functional recovery of the left ventricle after ischemia–reperfusion in Langendorff-perfused Nrf2-knockout mouse hearts

To examine the role of Nrf2 in the cardioprotective effect of 4-HNE, Nrf2-knockout mice were injected i.v. with either 4 mg/kg 4-HNE or vehicle, and 24 h later, the hearts were isolated and subjected to the same ischemia–reperfusion protocol. There was no difference in LV function before the induction of ischemia between the hearts from the Nrf2-knockout mice and those from the wild-type control mice. 4-HNE pretreatment did not affect the cardiac parameters at baseline in the Nrf2-knockout mice (data not shown). 4-HNE pretreatment did not improve the recovery of LVDP or rate-pressure product during reperfusion of the Nrf2-knockout mouse hearts. Moreover, 4-HNE pretreatment did not attenuate the total LDH activity released into the perfusate during reperfusion (Fig. 8). Notably, 4-HNE pretreatment

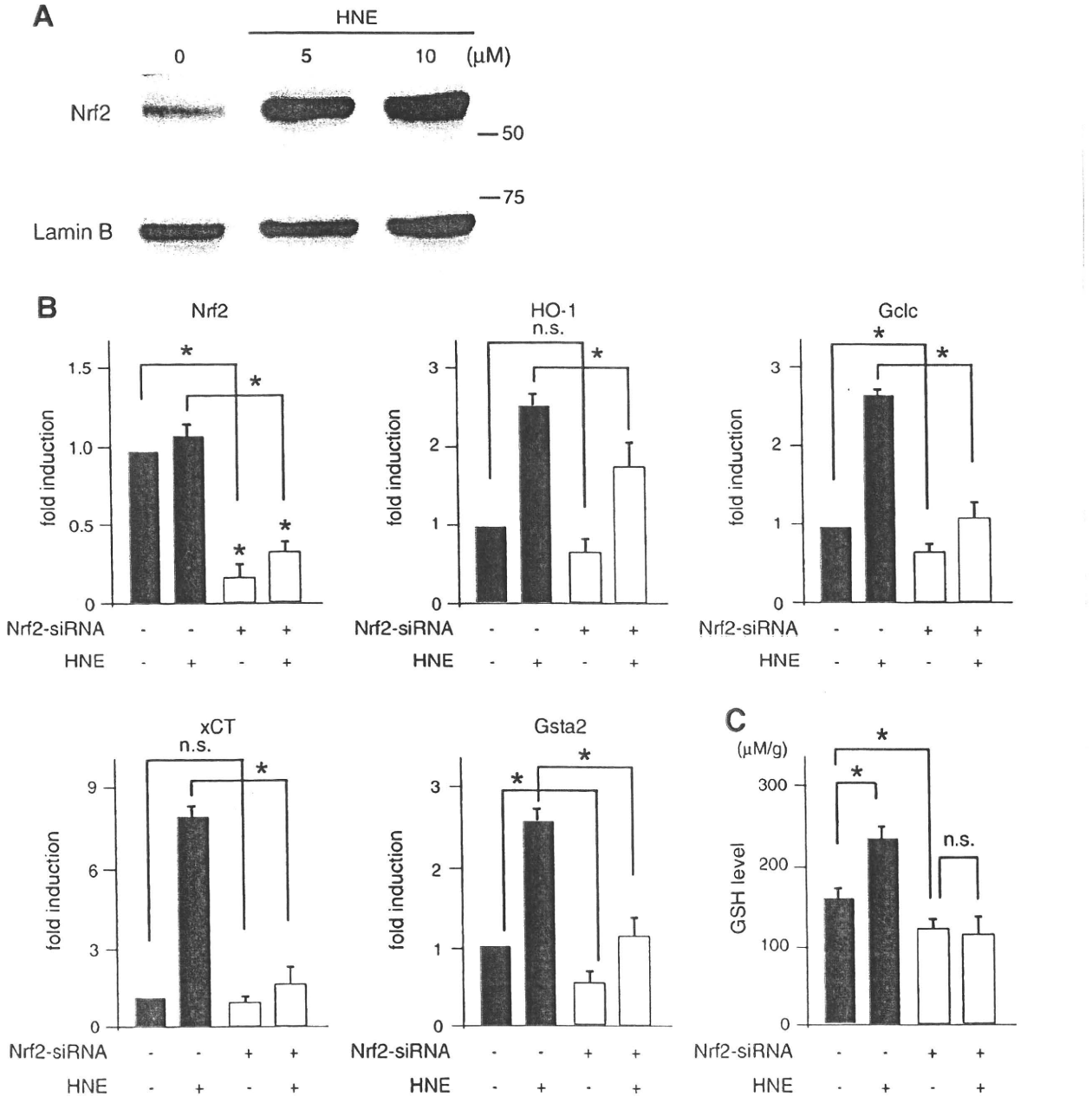

Fig. 4. Nrf2-dependent transcription is activated in 4-HNE-treated cardiomyocytes. (A) Cardiomyocytes were treated with sublethal concentrations of 4-HNE (0, 5, 10 μM) for 1 h. Nuclear extracts were subjected to SDS-PAGE, and Nrf2 was detected by immunoblotting. Membranes were stripped and reprobed with anti-Lamin B antibodies. (B) Cardiomyocytes were treated with either an Nrf2-specific siRNA or a control siRNA for 24 h, and then stimulated with 4-HNE (5 μM) for 6 h. Antioxidant gene expression was determined by Q-PCR analysis; $n=5$, $^*P<0.05$, compared to control siRNA-treated cardiomyocytes. (C) The intracellular levels of GSH were measured 14 h after 4-HNE (5 μM) treatment using Bioxytech GSH/GSSG-412 (Oxis Research), based on the Tietze method; $n=5$, $^*P<0.05$, compared to control siRNA-treated cardiomyocytes without 4-HNE stimulation.

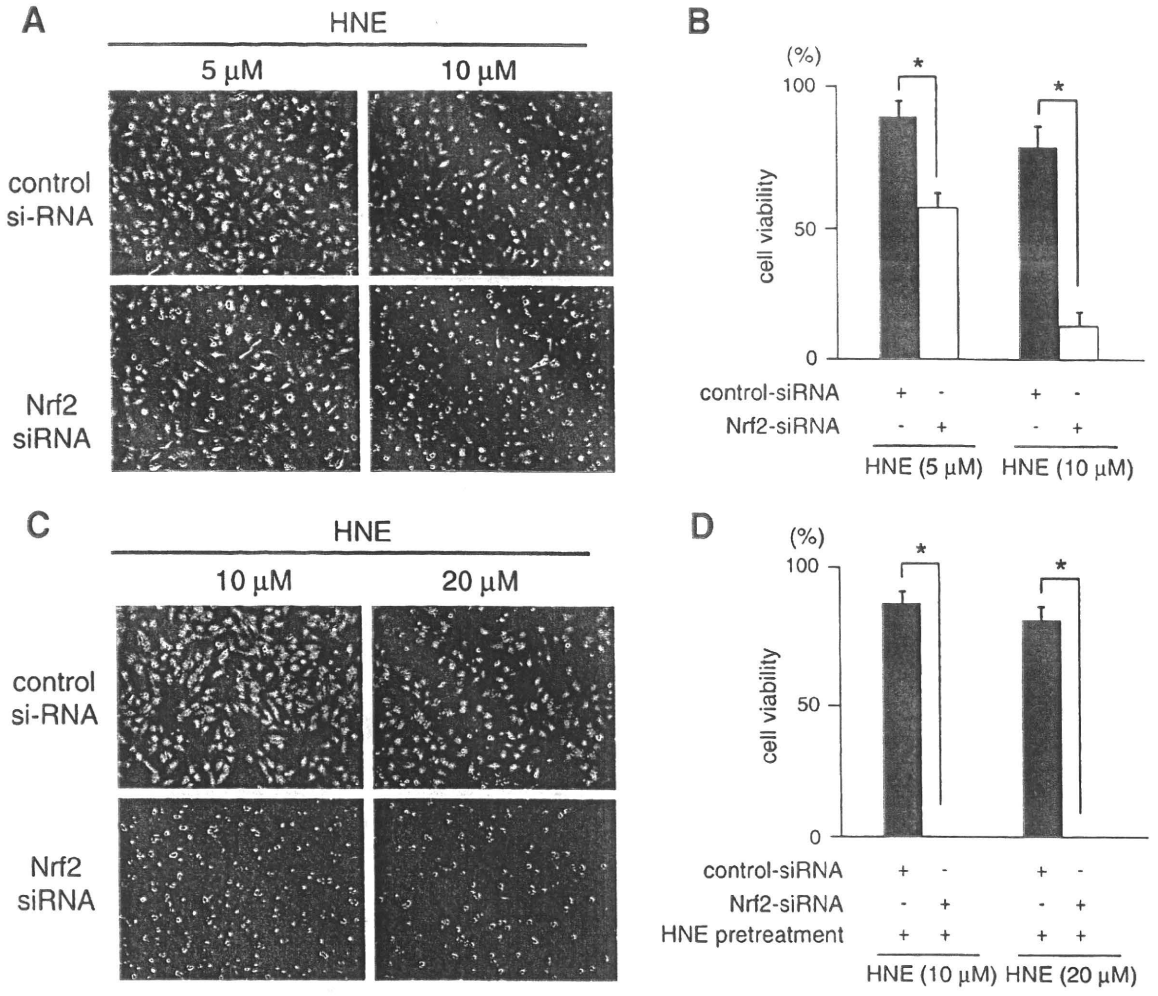

Fig. 5. Nrf2-deficient cardiomyocytes exhibit lower resistance to oxidative stress and the adaptive response to 4-HNE is completely abolished. Cardiomyocytes were treated with either Nrf2-specific siRNA or a control siRNA for 24 h, and then stimulated with 4-HNE (5 μM or 10 μM) for 24 h. (A) Representative images of cardiomyocytes after treatment with different concentrations of 4-HNE. (B) Quantification of cell viability. Data shown are mean ± SEM ($n = 5$). *$P<0.05$ vs. control siRNA-treated cardiomyocytes (unpaired Student's t-test). Nrf2-depleted cardiomyocytes were preincubated with 5 μM 4-HNE for 14 h, and then stimulated with 4-HNE (10 μM or 20 μM) for 24 h. (C) Representative images of cardiomyocytes after treatment with different concentrations of 4-HNE. (D) Quantification of cell viability. Data shown are mean ± SEM ($n = 5$). *$P<0.05$ vs. control siRNA-treated cardiomyocytes (unpaired Student's t-test).

increased the protein expression levels of xCT, GPX4, Gclc, Gsta, HO-1, and Catalase in the Nrf-2 wild-type hearts, but not in the Nrf2-knockout hearts (Supplemental Fig. 5).

4. Discussion

In addition to the pathogenic effects associated with oxidative stress, 4-HNE is considered to play an important role as a signal transduction molecule in stimulating the antioxidant defense network. This induction of stress-protective mechanisms is referred to as "stress-response hormesis" [9]. The present study provides insights into the clinical significance of stress-response hormesis induced by 4-HNE (Supplemental Fig. 7).

Hormesis is generally defined as a biphasic dose–response curve to a treatment that is beneficial at low levels but noxious at higher levels [15]. However, for practical reasons, most researchers in the fields of aging and molecular biology use a limited number of dosages within the optimal or hormetic zone when studying adaptive mechanisms. Thus, these researchers report hormetic effects without having to confirm the biphasic dose–response curve. This is certainly true for many examples of preconditioning. In the present study, we show a biphasic dose–response curve; 4-HNE induced cardiomyocyte death at higher concentrations (≥20 μM), whereas it had no appreciable cytotoxicity at lower concentrations (≤10 μM). Notably, a lower concentration of 4-HNE primed the cardiomyocytes for subsequent oxidative injury, thereby enabling the cells to adapt to cytotoxic concentrations of 4-HNE. Furthermore, we demonstrate that the administration of 4-HNE *via* the retro-orbital vein protects the heart against cell death induced by ischemia–reperfusion injury. 4-HNE pretreatment significantly attenuated the accumulation of 4-HNE adduct proteins during reperfusion. A growing body of evidence indicates that a brief ischemic insult in one organ releases endogenous factors that protect other organs against a prolonged ischemic insult [16]. This phenomenon is known as 'remote ischemic preconditioning'. The exact nature of signaling transduction from remote tissue to target organ remains to be fully elucidated. Aldehydes are more stable than their precursor ROS, which means that they can diffuse to sites at a distance from their site of injury. Aldehydes conjugate with receptive nucleophiles, such as glutathione. In the present study, we raise the possibility that aldehydes and/or their metabolites act as humoral mediators to mediate distant organ protection.

We show that Nrf2 is a key transcriptional regulator for 4-HNE-mediated establishment of antioxidative defenses, at least under acute conditions. These results are consistent with recent reports that

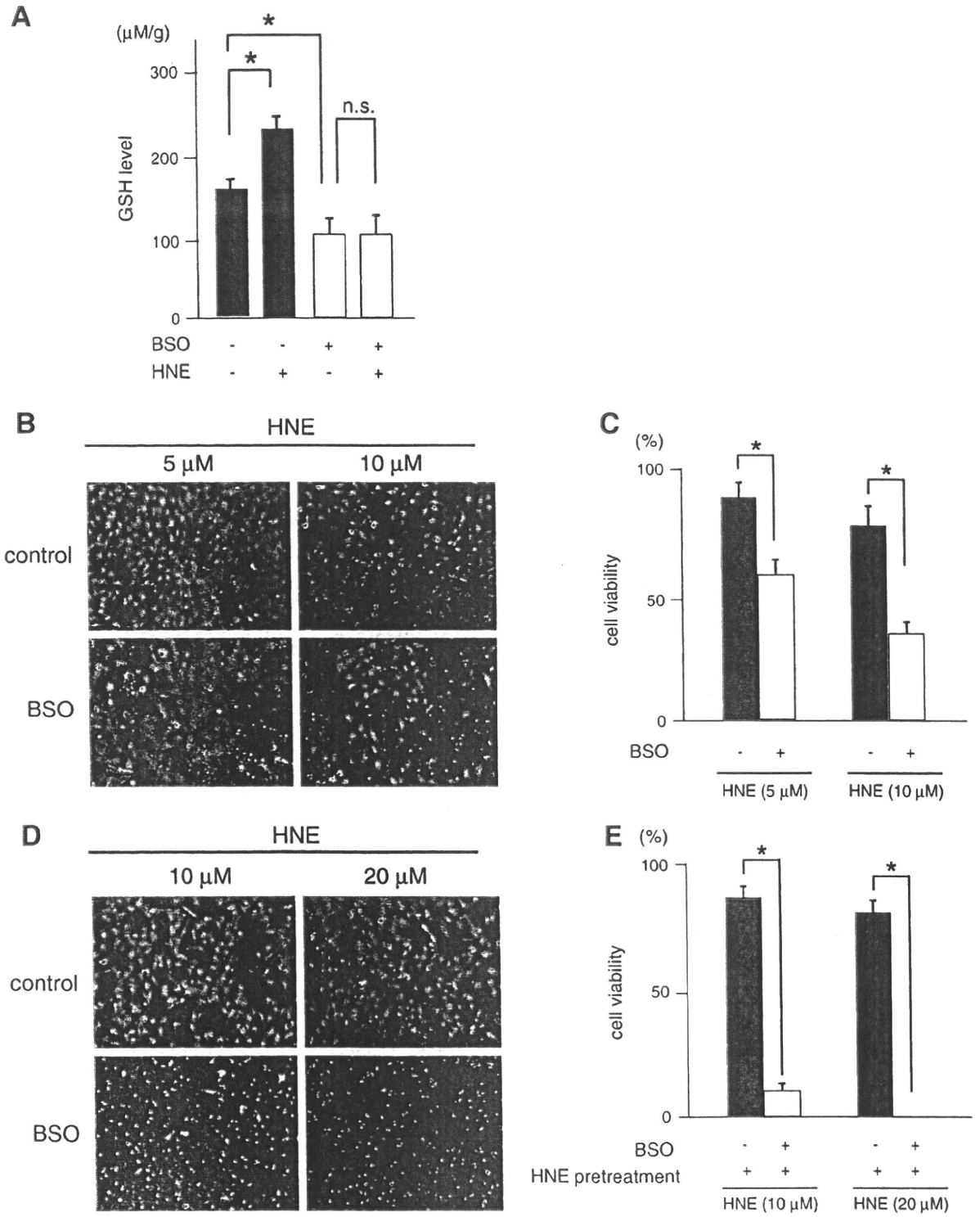

Fig. 6. Depletion of intracellular GSH using BSO renders cardiomyocytes less tolerant to 4-HNE and abolishes the 4-HNE-induced preconditioning effect. (A) Cardiomyocytes were incubated with 50 μM BSO in the presence or absence of 4-HNE (5 μM) for 14 h. The intracellular levels of GSH were measured using Bioxytech GSH/GSSG-412 (Oxis Research), based on the Tietze method; $n = 5$, $^*P<0.05$, compared to BSO-untreated cardiomyocytes without 4-HNE stimulation. (B) Cardiomyocytes were incubated with 50 μM BSO, and then stimulated with 4-HNE for 24 h. Representative images of cardiomyocytes after treatment with 4-HNE. (C) Quantification of cell viability. Data shown are mean ± SEM ($n = 5$). $^*P<0.05$ vs. BSO-untreated cardiomyocytes. (D) Cardiomyocytes were preconditioned with 4-HNE (5 μM) in the presence or absence of 50 μM BSO for 14 h, and then examined for tolerance to higher dosages (10 μM and 20 μM) of 4-HNE. Representative images of cardiomyocytes after treatment with 4-HNE. (E) Quantification of cell viability. Data shown are mean ± SEM ($n = 5$). $^*P<0.05$ vs. 4-HNE-preconditioned cardiomyocytes without BSO treatment.

Nrf2 signaling plays an important role in 3H-1,2-dithiole-3-thione (D3T)- or H_2O_2-induced protection against oxidative injury to cardiomyocytes [17] [18]. Under unstressed conditions, Nrf2 is tethered to Keap1 in the cytoplasm. This complex directs Nrf2 polyubiquitination and degradation. During oxidative stress, Nrf2 is liberated from Keap1 and enters the nucleus, where it forms a

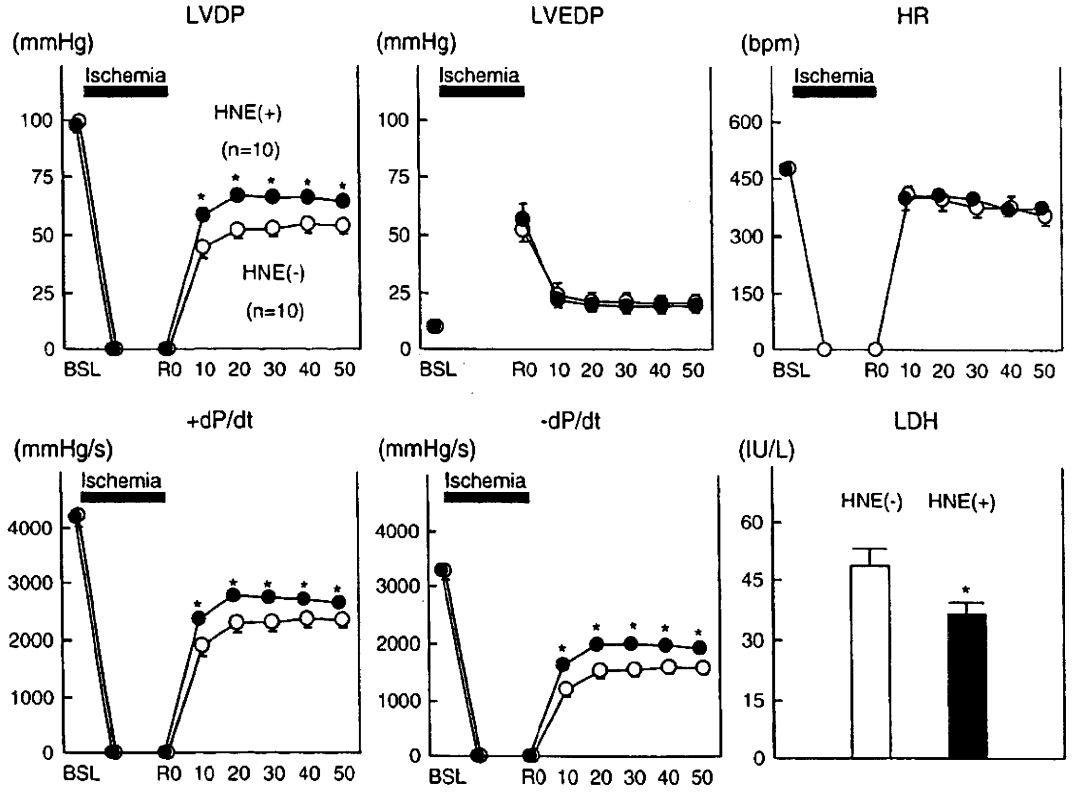

Fig. 7. 4-HNE treatment significantly improves the functional recovery of the left ventricle after ischemia-reperfusion in Langendorff-perfused hearts. The stock solution of 4-HNE was diluted with PBS, and a dose of 4 mg/kg HNE was administered via the retro-orbital vein 24 hours before sacrifice under anesthesia using diethyl ether. A vehicle solution (ethanol diluted with PBS) was administered in the same manner. Twenty-four hours later, the hearts were excised rapidly under deep anesthesia using pentobarbital and were immediately mounted on the Langendorff apparatus. Langendorff-perfused hearts were subjected to 25 min of total global ischemia, followed by aerobic reperfusion. LVDP, Recovery of left ventricular developing pressure; LVEDP, diastolic pressure; HR, heart rate; +/−dP/dt, peak positive/negative dP/dt; RPP, rate pressure product. *$P<0.05$ for HNE-preconditioned hearts ($n=10$) vs. control hearts ($n=10$) (unpaired Student's *t*-test).

heterodimer with the small Maf transcription factor Nrf2, to induce the expression of genes for proteins that function as antioxidants and enzymes that are involved in phase II detoxification and glutathione biosynthesis [14]. The mechanism by which 4-HNE induces the nuclear accumulation of Nrf2 remains to be clarified. Specific cysteine residues (Cys273/Cys288) in the Keap1 protein are known to act as a sensor for oxidative stress, and modification of these residues leads to a conformational change in Keap1, with consequent release of Nrf2 [19]. 4-HNE induces a conformational change in Keap1 directly *via* adduct formation or indirectly by increasing the production of mitochondrial ROS [20].

There is accumulating evidence that the myocardial GSH content influences susceptibility to ischemia–reperfusion injury [21]. N-acetylcysteine and γ-glutamyl-cysteine ethyl ester, which are precursors in glutathione biosynthesis, significantly attenuate myocardial ischemia–reperfusion injury when administered before reperfusion [22]. In contrast, glutathione depletion exacerbates myocardial ischemia–reperfusion injury [21,23]. We show that the stimulation of cellular GSH biosynthesis through the up-regulation of GCL, a rate-limiting enzyme in GSH biosynthesis, plays a crucial role in 4-HNE-mediated cardioprotection *via* Nrf2 activation. Reduction of the GSH content to about 100 μM/g by either Nrf2-siRNA or BSO (a GCL inhibitor) sensitized the cardiomyocytes to 4-HNE-induced death and completely abolished the cardioprotective effect of a low dose of 4-HNE.

In addition to Nrf2, activating transcription factor 4 (ATF4) is also activated following the induction of oxidative stress and GSH biosynthesis [24]. Recently, we reported that life-long mitochondrial oxidative stress increases the phosphorylation levels of the α-subunit of translation initiation factor 2 (eIF2α) [25]. Phosphorylation of eIF2α inhibits general protein synthesis, although it specifically stimulates the translation of ATF4. ATF4 stimulates the expression of genes that encode enzymes that are involved in serine biosynthesis, while it does not stimulate the expression of GCL. Serine is a precursor of glycine and cysteine, both of which are needed for the biosynthesis of GSH. ATF4 also stimulates the expression of the solute-like carrier family of amino acid transporters. Thus, ATF4 activates GSH biosynthesis by providing the amino acids necessary for glutathione biosynthesis.

The rate of GSH synthesis is determined primarily by GCL activity and the availability of precursor amino acids. In the acute setting, Nrf-2-dependent induction of GCL expression mainly contributes to the enhanced production of GSH, thereby replenishing the intracellular GSH pool. However, once the intracellular GSH is recovered to normal levels, GCL activity is subject to feedback inhibition by GSH. To maintain in the long-term the increased levels of GSH so as to re-establish homeostasis under persistent oxidative stress, cardiomyocytes shift their glucose metabolism from mitochondrial oxidative energy production to the generation of reducing equivalents (NADPH or GSH) in the cytosol by activating the pentose phosphate pathway and amino acid metabolism *via* an ATF4-dependent mechanism [25]. Thus, Nrf2 and ATF4 appear to act in a co-ordinated manner to regulate glutathione biosynthesis and the glutathione redox cycle at different time-points [26].

Although the baseline expression levels of catalase, Gclc, and Gsta were suppressed by up to 50% in the Nrf2-knockout hearts, as compared to the wild-type hearts (Zhang and Sano, unpublished observation), the Nrf2-knockout hearts were phenotypically normal under the unstressed condition. However, the preconditioning effect of 4-HNE was

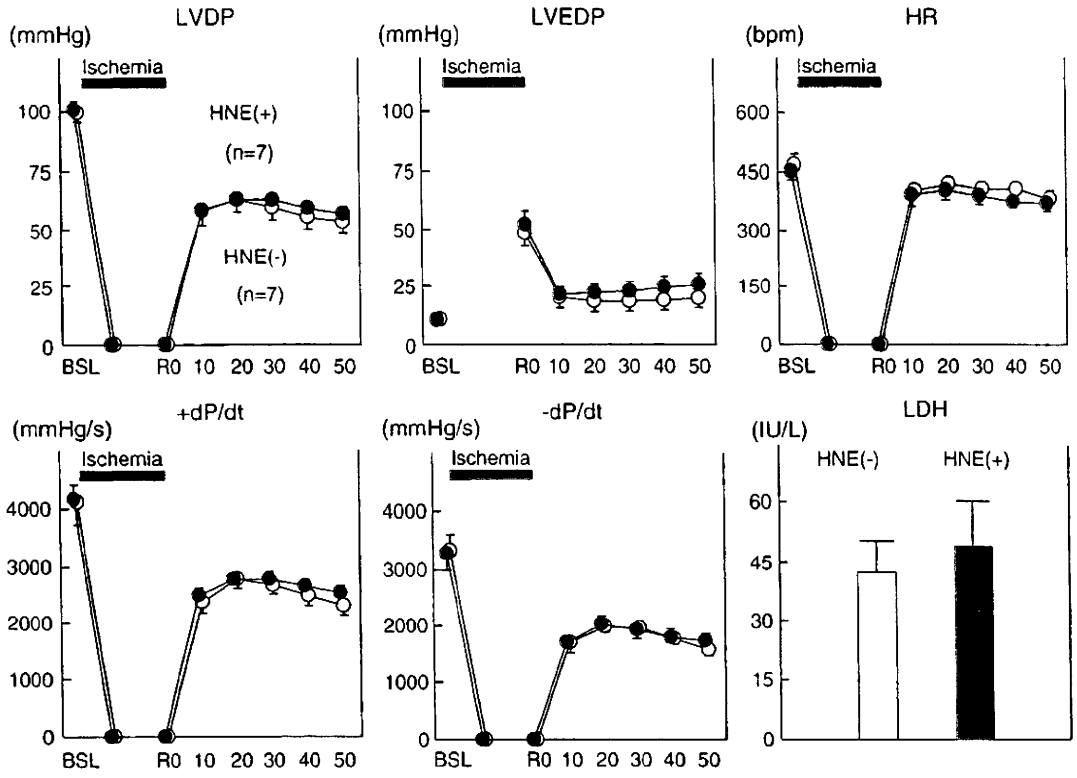

Fig. 8. 4-HNE treatment has no effect on the functional recovery of the left ventricle after ischemia–reperfusion in Langendorff-perfused Nrf2-knockout mouse hearts. 4-HNE (4 mg/kg) was injected into the ocular vein of each mouse. Langendorff-perfused hearts were subjected to 25 min of total global ischemia, followed by aerobic reperfusion. LVDP, Recovery of left ventricular developing pressure; LVEDP, diastolic pressure; HR, heart rate; +/−dP/dt, peak positive/negative dP/dt; RPP, rate pressure product. *$P<0.05$ for HNE-preconditioned ($n=7$) vs. control hearts ($n=7$) (unpaired Student's t-test).

completely absent in the Nrf2-knockout hearts. These results indicate that either Nrf2 is dispensable or that the Nrf2 defect is completely compensated for under the unstressed condition but is indispensable for the acute adaptive response under conditions of stress. Consistent with this notion, Nrf2-knockout hearts are prone to progression to terminal heart failure in response to pressure-overload by TAC [27]. Interestingly, the recovery of positive and negative dP/dt during early reperfusion was better in the Nrf2-knockout hearts than in the Nrf2-wildtype hearts (20 min of reperfusion and 10, 20, and 30 min of reperfusion, respectively) (Supplemental Fig. 4). The recovery of LVDP during early reperfusion tended to be better in Nrf2-KO mice, although the difference between Nrf2-wild-type and Nrf2-knockout mice was not statistically significant. These results strongly suggest that a compensatory mechanism against oxidative stress is stimulated in Nrf2-KO mice. However, the cardioprotection observed in the Nrf2-knockout mice was transient, and the recovery of LV function was similar in the two groups during late reperfusion (Supplemental Fig. 6). In addition, the finding that there was no difference in the total LDH activity released into the perfusate during reperfusion indicates that the extent of irreversible damage after ischemia–reperfusion is equivalent in Nrf2-wild-type and Nrf2-knockout mice, at least in these Langendorff-perfused hearts. 4-HNE pretreatment significantly improved the recovery of LV function during overall reperfusion, and attenuated LDH release during reperfusion in Nrf2-wildtype mice. Cardiac Nrf-2 was activated in the heart 60 min after the injection of 4-HNE via the retro-orbital vein. Both the up-regulation of cardiac anti-oxidant enzymes and the cardioprotection afforded by 4-HNE pretreatment were completely abrogated in the Nrf2- knockout mice. Therefore, we conclude that Nrf2 is essential for 4-HNE-induced cardioprotection, despite the differences in the patterns of LV functional recovery observed between Nrf2-wildtype and Nrf2-knockout mice. The mechanism by which Nrf2- knockout mice manifest improved LV function during early reperfusion remains unknown.

4-HNE is highly reactive so that most of 4-HNE may undergo nucleophilic addition reactions with electron-rich centers particularly non-protein and protein thiols and amines in the blood. Thus, we examined whether sufficient reactive 4-HNE reaches the heart upon systemic administration using antibodies specific for 4-HNE adduct proteins and showed that the level of 4-HNE in the heart was increased at 60 min after the administration of 4-HNE via the retro-orbital vein. We also demonstrated that cardiac Nrf2 is activated at 60 min after systemic administration of 4-HNE. We concluded that 4-HNE or 4-HNE conjugate metabolite can reaches the heart upon systemic administration and stimulate intracellular signaling in the heart. Notably, not only free 4-HNE but also 4-HNE conjugate metabolite can stimulate intracellular signaling and increased cell growth in cultured vascular smooth muscle cells [28].

Several studies have suggested that the generation of aldehydes, such as 4-HNE, contributes to much of the damage induced by ROS [29]. The present study intriguingly shows that a sublethal concentration of 4-HNE protects cardiomyocytes from ischemia–reperfusion injury. An improved understanding of the dual roles of 4-HNE would facilitate the design of novel strategies for cardioprotection against oxidative stress [30].

Disclosures

None.

Sources of funding

This work was supported by the Japan-China Medical Association (to Y.Z.) and by a PRESTO (Metabolism and Cellular Function) grant from the Japanese Science and Technology Agency (to M.S.).

Acknowledgments

The authors thank the Japan-China Medical Association and the Japan Foundation for giving Y. Zhang the opportunity to join our laboratory. The authors thank Y. Miyake, H. Shiozawa, M. Abe, and M. Doi for technical assistance. M. Sano and M. Suematsu are core members of the Global Center of Excellence (GCOE) for Human Metabolomics Systems Biology at MEXT.

Appendix A. Supplementary data

Supplementary data associated with this article can be found, in the online version, at doi:10.1016/j.yjmcc.2010.05.011.

References

[1] Conklin D, Prough R, Bhatanagar A. Aldehyde metabolism in the cardiovascular system. Mol Biosyst 2007 Feb;3(2):136–50.
[2] Watson AD, Leitinger N, Navab M, Faull KF, Horkko S, Witztum JL, et al. Structural identification by mass spectrometry of oxidized phospholipids in minimally oxidized low density lipoprotein that induce monocyte/endothelial interactions and evidence for their presence in vivo. J Biol Chem 1997 May 23;272 (21):13597–607.
[3] Liu Q, Raina AK, Smith MA, Sayre LM, Perry G. Hydroxynonenal, toxic carbonyls, and Alzheimer disease. Mol Aspects Med Aug-Oct 2003;24(4-5):305–13.
[4] Chen CH, Budas GR, Churchill EN, Disatnik MH, Hurley TD, Mochly-Rosen D. Activation of aldehyde dehydrogenase-2 reduces ischemic damage to the heart. Science 2008 Sep 12;321(5895):1493–5.
[5] Honarbakhsh S, Schachter M. Vitamins and cardiovascular disease. Br J Nutr 2009 Apr;101(8):1113–31.
[6] Uchida K, Shiraishi M, Naito Y, Torii Y, Nakamura Y, Osawa T. Activation of stress signaling pathways by the end product of lipid peroxidation. 4-hydroxy-2-nonenal is a potential inducer of intracellular peroxide production. J Biol Chem 1999 Jan 22;274(4):2234–42.
[7] Dickinson DA, Iles KE, Watanabe N, Iwamoto T, Zhang H, Krzywanski DM, et al. 4-hydroxynonenal induces glutamate cysteine ligase through JNK in HBE1 cells. Free Radic Biol Med 2002 Oct 1;33(7):974.
[8] Chen ZH, Saito Y, Yoshida Y, Sekine A, Noguchi N, Niki E. 4-Hydroxynonenal induces adaptive response and enhances PC12 cell tolerance primarily through induction of thioredoxin reductase 1 via activation of Nrf2. J Biol Chem 2005 Dec 23;280(51):41921–7.
[9] Gems D, Partridge L. Stress-response hormesis and aging: "that which does not kill us makes us stronger". Cell Metab 2008 Mar;7(3):200–3.
[10] Iida K, Itoh K, Kumagai Y, Oyasu R, Hattori K, Kawai K, et al. Nrf2 is essential for the chemopreventive efficacy of oltipraz against urinary bladder carcinogenesis. Cancer Res 2004 Sep 15;64(18):6424–31.
[11] Tokudome S, Sano M, Shinmura K, Matsuhashi T, Morizane S, Moriyama H, et al. Glucocorticoid protects rodent hearts from ischemia/reperfusion injury by activating lipocalin-type prostaglandin D synthase-derived PGD2 biosynthesis. J Clin Invest 2009 Jun;119(6):1477–88.
[12] Hyafil F, Vergely C, Du Vignaud P, Grand-Perret T. In vitro and in vivo reversal of multidrug resistance by GF120918, an acridonecarboxamide derivative. Cancer Res 1993 Oct 1;53(19):4595–602.
[13] Kettner A, Kumar L, Anton IM, Sasahara Y, de la Fuente M, Pivniouk VI, et al. WIP regulates signaling via the high affinity receptor for immunoglobulin E in mast cells. J Exp Med 2004 Feb 2;199(3):357–68.
[14] Motohashi H, Yamamoto M. Nrf2-Keap1 defines a physiologically important stress response mechanism. Trends Mol Med 2004 Nov;10(11):549–57.
[15] Calabrese EJ, Baldwin LA, Holland CD. Hormesis: a highly generalizable and reproducible phenomenon with important implications for risk assessment. Risk Anal 1999 Apr;19(2):261–81.
[16] Kharbanda RK, Nielsen TT, Redington AN. Translation of remote ischaemic preconditioning into clinical practice. Lancet 2009 Oct 31;374(9700):1557–65.
[17] Zhu H, Jia Z, Misra BR, Zhang L, Cao Z, Yamamoto M, et al. Nuclear factor E2-related factor 2-dependent myocardiac cytoprotection against oxidative and electrophilic stress. Cardiovasc Toxicol Summer 2008;8(2):71–85.
[18] Purdom-Dickinson SE, Lin Y, Dedek M, Morrissy S, Johnson J, Chen QM. Induction of antioxidant and detoxification response by oxidants in cardiomyocytes: evidence from gene expression profiling and activation of Nrf2 transcription factor. J Mol Cell Cardiol 2007 Jan;42(1):159–76.
[19] Kobayashi A, Kang MI, Watai Y, Tong KI, Shibata T, Uchida K, et al. Oxidative and electrophilic stresses activate Nrf2 through inhibition of ubiquitination activity of Keap1. Mol Cell Biol 2006 Jan;26(1):221–9.
[20] Hill BG, Dranka BP, Zou L, Chatham JC, Darley-Usmar VM. Importance of the bioenergetic reserve capacity in response to cardiomyocyte stress induced by 4-hydroxynonenal. Biochem J 2009 Nov 15;424(1):99–107.
[21] Singh A, Lee KJ, Lee CY, Goldfarb RD, Tsan MF. Relation between myocardial glutathione content and extent of ischemia–reperfusion injury. Circulation 1989 Dec;80(6):1795–804.
[22] Hoshida S, Kuzuya T, Yamashita N, Nishida M, Kitahara S, Hori M, et al. gamma-Glutamylcysteine ethyl ester for myocardial protection in dogs during ischemia and reperfusion. J Am Coll Cardiol 1994 Nov 1;24(5):1391–7.
[23] Blaustein A, Deneke SM, Stolz RI, Baxter D, Healey N, Fanburg BL. Myocardial glutathione depletion impairs recovery after short periods of ischemia. Circulation 1989 Nov;80(5):1449–57.
[24] Harding HP, Zhang Y, Zeng H, Novoa I, Lu PD, Calfon M, et al. An integrated stress response regulates amino acid metabolism and resistance to oxidative stress. Mol Cell 2003 Mar;11(3):619–33.
[25] Endo J, Sano M, Katayama T, Hishiki T, Shinmura K, Morizane S, et al. Metabolic remodeling induced by mitochondrial aldehyde stress stimulates tolerance to oxidative stress in the heart. Circ Res 2009 Nov 20;105(11):1118–27.
[26] Sano M, Fukuda K. Activation of mitochondrial biogenesis by hormesis. Circ Res 2008 Nov 21;103(11):1191–3.
[27] Li J, Ichikawa T, Villacorta L, Janicki JS, Brower GL, Yamamoto M, et al. Nrf2 protects against maladaptive cardiac responses to hemodynamic stress. Arterioscler Thromb Vasc Biol Jul 10 2009.
[28] Ramana KV, Bhatnagar A, Srivastava S, Yadav UC, Awasthi S, Awasthi YC, et al. Mitogenic responses of vascular smooth muscle cells to lipid peroxidation-derived aldehyde 4-hydroxy-trans-2-nonenal (HNE): role of aldose reductase-catalyzed reduction of the HNE-glutathione conjugates in regulating cell growth. J Biol Chem 2006 Jun 30;281(26):17652–60.
[29] Veronneau M, Comte B, Des Rosiers C. Quantitative gas chromatographic-mass spectrometric assay of 4-hydroxynonenal bound to thiol proteins in ischemic/reperfused rat hearts. Free Radic Biol Med 2002 Nov 15;33(10):1380–8.
[30] Hill BG, Bhatnagar A. Beyond reactive oxygen species: aldehydes as arbitrators of alarm and adaptation. Circ Res 2009 Nov 20;105(11):1044–6.

Am J Physiol Heart Circ Physiol 299: H1795–H1804, 2010.
First published September 17, 2010; doi:10.1152/ajpheart.00001.2010.

Increased C-reactive protein expression exacerbates left ventricular dysfunction and remodeling after myocardial infarction

Toshiyuki Takahashi, Toshihisa Anzai, Hidehiro Kaneko, Yoshinori Mano, Atsushi Anzai, Toshiyuki Nagai, Takashi Kohno, Yuichiro Maekawa, Tsutomu Yoshikawa, Keiichi Fukuda, and Satoshi Ogawa

Division of Cardiology, Department of Medicine, Keio University School of Medicine, Tokyo, Japan

Submitted 4 January 2010; accepted in final form 15 September 2010

Takahashi T, Anzai T, Kaneko H, Mano Y, Anzai A, Nagai T, Kohno T, Maekawa Y, Yoshikawa T, Fukuda K, Ogawa S. Increased C-reactive protein expression exacerbates left ventricular dysfunction and remodeling after myocardial infarction. *Am J Physiol Heart Circ Physiol* 299: H1795–H1804, 2010. First published September 17, 2010; doi:10.1152/ajpheart.00001.2010.—We previously reported serum C-reactive protein (CRP) elevation after acute myocardial infarction (MI) to be associated with adverse outcomes including cardiac rupture, left ventricular (LV) remodeling, and cardiac death. Experimental studies have indicated that CRP per se has various biological actions including proinflammatory and proapoptotic effects, suggesting a pathogenic role of CRP in the post-MI remodeling process. We tested the hypothesis that increased CRP expression would exacerbate adverse LV remodeling after MI via deleterious effects of CRP. Transgenic mice with human CRP expression (CRP-Tg) and their transgene-negative littermates (control) underwent left coronary artery ligation. There was no apparent difference in phenotypic features between CRP-Tg and control mice before MI. Although mortality and infarct size were similar in the two groups, CRP-Tg mice showed more LV dilation and worse LV function with more prominent cardiomyocyte hypertrophy and fibrosis in the noninfarcted regions after MI than controls. Histological evaluation conducted 1 wk post-MI revealed a higher rate of apoptosis and more macrophage infiltration in the border zones of infarcted hearts from CRP-Tg mice in relation to increased monocyte chemotactic protein (MCP)-1 expression and matrix metalloproteinase (MMP)-9 activity. Increased CRP expression exacerbates LV dysfunction and promotes adverse LV remodeling after MI in mice. The deleterious effect of CRP on post-MI LV remodeling may be associated with increased apoptotic rates, macrophage infiltration, MCP-1 expression, and MMP-9 activity in the border zone.

macrophage; apoptosis

EARLY REVASCULARIZATION AND pharmacological therapy have been used to improve clinical outcomes in patients with acute myocardial infarction (MI). However, in some instances, particularly in those in which myocardial ischemic damage is too severe and extensive to allow salvage, adverse left ventricular (LV) remodeling develops following MI. This deleterious remodeling is characterized by progressive LV dilation and depressed LV function. In the long-term, the development of LV remodeling leads to detrimental outcomes such as congestive heart failure and lethal arrhythmias. Although the precise mechanisms underlying adverse LV remodeling remain to be determined, the inflammatory response to myocardial tissue damage plays a pivotal role in the pathophysiology of the remodeling process (8).

C-reactive protein (CRP) is a major acute-phase inflammatory reactant produced predominantly in the liver. We previously reported that marked serum CRP elevation after acute MI is associated with adverse outcomes such as cardiac rupture, LV remodeling, LV mural thrombosis, and cardiac death (2, 3, 29). In addition, the CRP level in the acute phase of MI is a powerful independent marker of heart failure and long-term mortality (28). Although the CRP level is reportedly a significant risk factor for cardiovascular disease (23, 24), CRP has been regarded as simply a prognostic marker in clinical settings. However, recent experimental studies have indicated that CRP per se has various biological actions, including proinflammatory, thrombogenic, atherogenic, and proapoptotic effects (6, 7, 9, 10, 22, 26, 32, 33), suggesting a pathogenic role of CRP in the inflammatory response and myocardial tissue damage associated with LV remodeling after MI. Therefore, we hypothesized that increased CRP expression would have deleterious effects on adverse LV remodeling after MI.

To examine the direct in vivo involvement of CRP in the adverse remodeling process following MI, we generated transgenic mice with human CRP expression (CRP-Tg). Large anterior wall MIs were then induced in CRP-Tg mice and their transgene-negative littermates. We assessed survival, infarct size, and LV size and function after MI. We then sought to determine the mechanisms by which increased CRP expression might accelerate adverse LV remodeling after MI.

METHODS

Generation and characterization of CRP-Tg mice. The study protocol was approved by the Institutional Animal Care and Use Committee at Keio University School of Medicine (No. 050015), and animal use and care were in accordance with Institutional and National Institutes of Health (NIH) guidelines. To generate transgenic mice with ubiquitous expression of human CRP, human CRP cDNA was inserted into the unique *Eco*RI site between the CAG (modified chicken β-actin promoter with CMV-IE enhancer) promoter and 3′-flanking sequence of the rabbit β-globin gene of the pCAGGS expression vector 4797 (Fig. 1*A*). The pronuclei of fertilized eggs from hyperovulated C57BL/6 mice were microinjected with this DNA construct. Founder animals were identified and crossbred with wild-type mice of the same strain. Gene presence was confirmed using genomic DNA purified from clipped tail tips (Fig. 1*B*); gene expression in the heart was confirmed by real-time RT-PCR with primers for human CRP (forward: GCTGGTTATTGTGCTGTCTC; reverse: CAGTTCAGGACATTAGGACTGAAG). Protein expression of human CRP in the heart was also confirmed by Western blotting of LV homogenates with antibodies recognizing human CRP (Sigma-Aldrich, St. Louis, MO; Fig. 1*C*). Human CRP expression in various organ tissues, including heart, lung, and liver, was determined by

Address for reprint requests and other correspondence: T. Anzai, Div. of Cardiology, Dept. of Medicine, Keio Univ. School of Medicine, 35 Shinanomachi, Shinjuku-ku, Tokyo 160-8582, Japan (e-mail: anzai@cpnet.med.keio.ac.jp).

immunohistochemistry (Fig. 1*D*). Blood sampling was taken, and the serum was stored at −80°C when animals were euthanized. Serum CRP levels were measured by latex agglutination immunoassay using the Nanopia CRP kit (Sekisui Medical, Tokyo, Japan). The detection limit of this assay was 0.1 ml/dL. Blood pressures were measured in awake animals by the tail-cuff method using the BP-98A system (Softron; Tokyo, Japan). Mice were housed with free access to food and water and exposed to 12-h:12-h light-dark cycles.

MI. Male CRP-Tg mice (3 to 4 mo old; $n = 59$) and their age-matched, male transgene-negative littermates (control; $n = 63$) were used for the study. MI was induced by permanent ligation of the left coronary artery as described previously (13, 30). Briefly, mice were anesthetized with ketamine and xylazine, intubated, and connected to a rodent ventilator. The chest cavity was opened through the fourth intercostal space to expose the heart. Suture (7-0 silk) was tied around the proximal left coronary artery. Complete occlusion of the vessel was confirmed by the presence of myocardial blanching in the perfusion bed, and subsequently by histological assessment.

Survival study. MIs were induced in the CRP-Tg and control mice in a randomized, blinded fashion. This study was designed to determine the 5-wk survival of mice following MI; therefore, mice that did not survive the surgical procedure were not included in the analysis.

Histology. After hearts were arrested in diastole, excised, and rinsed with saline, they were fixed in Formalin and embedded in paraffin. The sections from apex, mid-LV, and base were stained with hematoxylin and eosin and Masson's trichrome. Infarct size was determined as the mean percent of infarct lengths divided by total LV circumferences in the three sections. Myocyte hypertrophy in the noninfarcted septum was assessed by measuring the mean myocyte cross-sectional area. The percent area of fibrosis within the remote and MI regions of the LV was also computed. In a subset of mice euthanized at 1 and 5 wk after MI, the atria and right ventricle were removed from the heart and the LV was opened by a long-axis incision. The LV was then laid flat on the plate. The endocardial and epicardial surfaces were photographed by a digital camera. Infarct size was measured as the ratio of infarct area to total LV area by planimetry as previously described (4). Infarct size was also assessed in a subgroup of animals euthanized at 24 h after MI to avoid differences in hypertrophy of the noninfarcted wall that might result from differences in human CRP expression. Hearts were excised and immersed in 1% agarose and sectioned perpendicular to the long axis into 1-mm-thick slices and stained with 1.0% 2,3,5-triphenyltetrazolium chloride (TTC) for 10 min at 37°C to delineate the infarct area from the noninfarcted viable area. Each slice was weighed and photographed, and the LV area and the area of infarction for each slice were determined by planimetry as described previously (30).

Echocardiography. Echocardiography was performed with a 12-MHz probe (EnVisor; Philips Medical Systems, Andover, MA) in mice before MI and 1 or 5 wk after MI. Animals were anesthetized with an intraperitoneal injection of tribromoethanol (125 μg/g). A parasternal short-axis view was obtained as a guide for LV M-mode imaging at the papillary muscle level. LV dimensions, including end-diastole diameter, end-systole diameter, and wall thickness, were measured using the leading-edge method on three consecutive cardiac cycles. The LV ejection fraction (EF) was calculated using the area-length method as described previously (30).

Hemodynamics. LV pressure was measured in intact mice 5 wk after MI ($n = 10$ for the control group; $n = 9$ for the CRP-Tg group). Mice were anesthetized with an intraperitoneal injection of pentobarbital sodium (80 μg/g) and connected to a rodent ventilator after endotracheal intubation. A 1.4F micromanometer catheter (Millar Instruments, Houston, TX) was inserted via the right carotid artery and advanced into the LV. Peak rates of LV pressure development (LV $+dP/dt$) and relaxation (LV $-dP/dt$) were measured using analysis software (PowerLab; ADInstruments, Colorado Springs, CO). Ten sequential beats were averaged for each measurement.

TUNEL staining. To evaluate the extent of apoptosis in infarcted hearts, TUNEL assays were performed on sectioned LV samples using the CardioTACS In Situ Apoptosis Detection Kit (R&D Systems, Minneapolis, MN) as previously described (30). Images of six to eight contiguous sections across the LV wall were obtained at the midventricle level to measure the number of TUNEL-positive cardiac myocyte nuclei in the noninfarcted remote, peri-infarct border, and infarct zones. Digital images were evaluated using NIH Image to count TUNEL-positive stained nuclei and the total number of nuclei in a nuclease pretreated section from the same region. The area of each section was planimetered to calculate the average density of nuclei (nuclei per squared micrometers), the TUNEL-positive stained nuclei (per squared micrometers), and the rate of TUNEL-positive nuclei (per 10^5 nuclei).

Quantitative real-time PCR. Total RNA was isolated by acid-phenol extraction in the presence of chaotropic salts (TRIzol; Invitrogen, Carlsbad, CA) and subsequent isopropanol-ethanol precipitation as described previously (18, 27). Real-time RT-PCR of each sample was carried out with a TaqMan RNA PCR kit and ABI Prism 7500 Sequence Detection System (Applied Biosystems, Foster City, CA) according to the manufacturer's protocol. Expression of the housekeeping gene GAPDH was used for normalization. Bcl-2, Bcl-xL, Bax, and Bad assays were purchased as preoptimized kits from Applied Biosystems.

Immunohistochemical studies. Immunohistochemical studies were performed employing immunoperoxidase methods (18, 20). Hearts were fixed in Formalin, embedded in paraffin, and cut into 5-μm-thick cross sections. The sections were stained with antibodies against F4/80 (Novus Biological, Littleton, CO; dilution 1:50) for monocyte-derived macrophages, monocyte chemotactic protein (MCP)-1 (Hycult Biotech; Uden, The Netherlands; dilution 1:50), matrix metalloproteinase (MMP)-9 (Abcam, Cambridge, MA; dilution 1:100), and human CRP (Epitomics; Burlingame, CA; dilution 1:100). Because antibodies against neutrophils (Abcam; dilution 1:100) crossreacted with phagocytic macrophages, neutrophils were counted in the sections stained with hematoxylin and eosin by morphological assessment. For quantitative analysis, the number of positive cells was counted per field for five random fields and expressed as the number per squared millimeters.

Western blot analysis. LV samples were homogenized with lysis buffer containing 1% Triton X-100 and protease inhibitors. After centrifugation at 16,000 *g* for 30 min at 4°C, the supernatants were collected. Western blot analysis was performed as previously described (30). Equal quantities of proteins from LV samples were loaded on gels. Antibodies to MCP-1 (Abcam) and uncleaved and cleaved caspase-3 (Cell Signaling Technology, Danvers, MA) were used. After membranes were probed with primary antibodies, they were stripped of bound immunoglobulins and reprobed with anti-mouse GAPDH (Santa Cruz Biotechnology, Santa Cruz, CA) to correct for protein loading. The bands on the X-ray film were quantified by scanning densitometry with the ImageJ software and expressed as a percentage of the control.

Zymography. Gelatin zymography was performed to assess the activities of MMP-2 and MMP-9. Equal volumes of tissue extract from LV samples (10 μg of protein) were loaded on 10% SDS-polyacrylamide gels containing 1 mg/ml of gelatin (Novex Zymogram Gels; Invitrogen). The gels were incubated in renaturing buffer (2.5% Triton X-100) and then incubated in developing buffer at 37°C for 24 h (50 mM Tris·HCl, 10 mM $CaCl_2$). The gels were stained with 0.5% Coomassie Blue. Areas of protease activity appear as clear bands against a dark blue background where the protease has digested the gelatin substrate.

Serum MCP-1 measurement. Serum MCP-1 levels were measured by quantitative sandwich enzyme immunoassay technique using the Quantikine kit (R&D Systems) according to the manufacturer's instruction.

Table 1. *Morphometric data of control and CRP-Tg mice non-MI and post-MI*

	Non-MI		Post-MI		
	Control	CRP-Tg	Control	CRP-Tg	ANOVA
n	8	8	14	14	
BW, g	28.8 ± 2.3	28.0 ± 2.1	30.2 ± 3.1	29.4 ± 3.8	ns
LV + RV, mg	118 ± 13	112 ± 8	158 ± 15*	182 ± 14*†	$P < 0.0001$
(LV + RV)/BW, mg/g	4.1 ± 0.4	4.0 ± 0.4	5.3 ± 0.7*	6.3 ± 0.9*†	$P < 0.0001$
Lung, mg	160 ± 21	161 ± 12	174 ± 16	203 ± 31*†	$P = 0.0001$
Lung/BW, mg/g	5.6 ± 0.7	5.8 ± 0.5	5.8 ± 0.8	7.0 ± 1.4*†	$P = 0.003$
Liver, mg	1,285 ± 171	1,244 ± 153	1,199 ± 91	1,176 ± 153	ns
Liver/BW, mg/g	44.8 ± 5.6	44.5 ± 4.3	40.0 ± 3.8	40.2 ± 4.6	$P = 0.02$

Values are means ± SD; *n*, number of animals studied. CRP-Tg, transgenic mice with human C-reactive protein expression; MI, myocardial infarction; BW, body weight; LV, left ventricle; RV, right ventricle; ns, not significant. *$P < 0.05$, non-MI vs. post-MI; †$P < 0.05$, post-MI CRP-Tg vs. post-MI control (Bonferroni's test).

Statistical analysis. Results are presented as counts or means ± SD. Group comparisons were made using the Student's *t*-test (two tailed), the Mann-Whitney U test or the one-way ANOVA with Bonferroni's post hoc test for continuous data. Survival curves were computed using the Kaplan-Meier method and compared using the log rank test. The null hypothesis was rejected if $P < 0.05$. Analyses were performed using the GraphPad Prism (GraphPad software; San Diego, CA).

RESULTS

Characterization of CRP-Tg. There were no differences in phenotypic features including general appearance, body weight, and organ weights between control and CRP-Tg mice in the non-MI setting (Table 1). Systolic blood pressures measured by the tail-cuff method were similar in control and

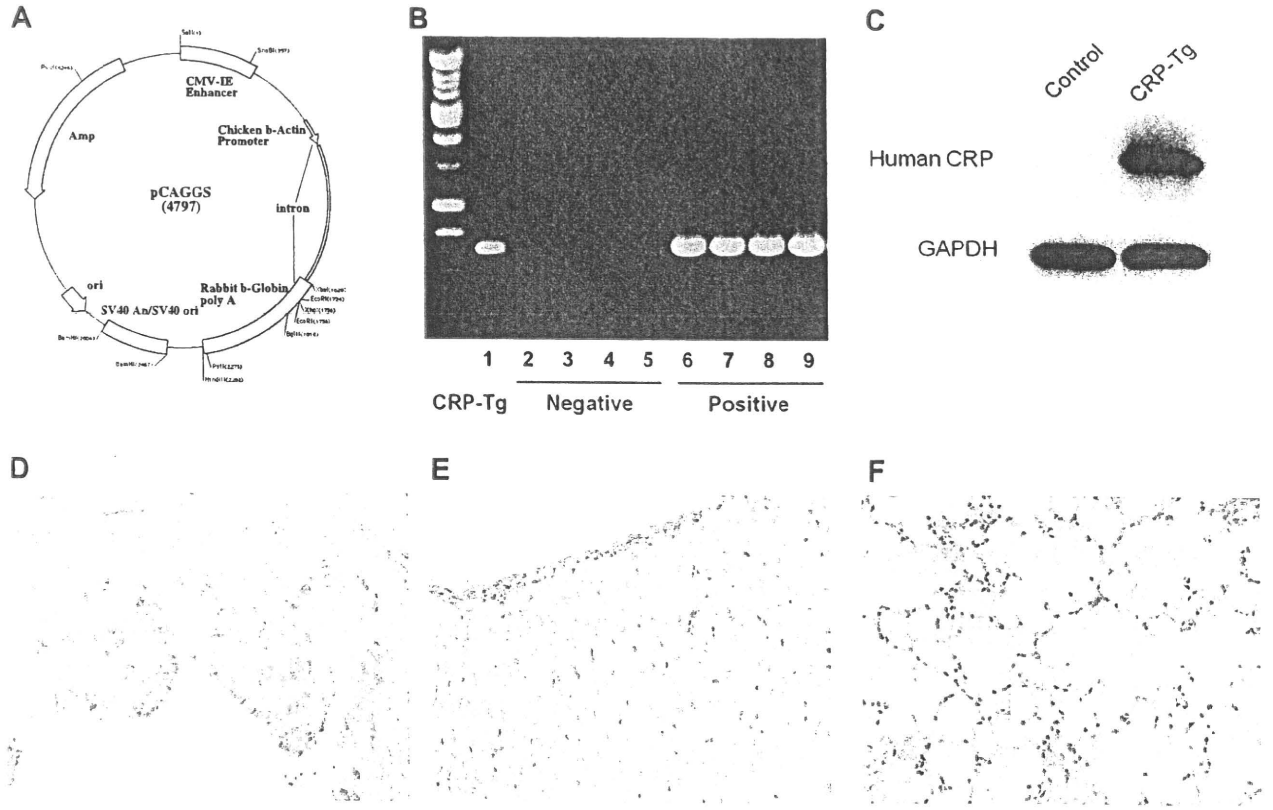

Fig. 1. Generation and characterization of transgenic mice with human C-reactive protein (CRP) expression (CRP-Tg) mice. *A*: human CRP cDNA was inserted into the unique *Eco*RI site between the CAG (modified chicken β-actin promoter with CMV-IE enhancer) promoter and 3′-flanking sequence of the rabbit β-globin gene of the pCAGGS expression vector. *B*: gene expression was confirmed by RT-PCR using genomic DNA extracted from clipped tails. *Lane 1* is the positive control. *Lanes 2-5* are samples negative for the CRP transgene, and *lanes 6-9* from positive samples. *C*: Western blotting of left ventricular (LV) homogenates showed marked protein expression of human CRP in LV samples from CRP-Tg mice but not in those from control mice. *D–F*: immunohistochemical studies confirmed local expression of human CRP (stained in brown) in sections from heart (*D*, 200×), liver (*E*, 400×), and lung (*F*, 400×).

CRP-Tg mice before MI (control, 106 ± 6 mmHg; CRP-Tg, 105 ± 9 mmHg, n = 10 for each group; P = 0.77). Heart rates were also similar in control and CRP-Tg mice (control, 574 ± 84 beats/min; CRP-Tg, 575 ± 56 beats/min, n = 10 for each group; P = 0.96). Serum CRP levels were 32 ± 7 mg/l in non-MI CRP-Tg mice (n = 8), whereas CRP was undetectable in serum from control mice. Histological examination in the hearts from CRP-Tg mice identified cardiac myocytes and endothelial cells as a main source of human CRP (Fig. 1*D*). No pathological abnormalities such as inflammation, hypertrophy, and fibrosis were seen in the hearts from non-MI CRP-Tg mice, which were indistinguishable from those from control mice. The count of neutrophils in the hearts was not different between control and CRP-Tg mice (control, 15 ± 6 cells/mm^2; CRP-Tg, 16 ± 6 cells/mm^2, n = 6 for each group; P = 0.81). The count of macrophages in the hearts was also comparable between the two groups (control, 4 ± 4 cells/mm^2; CRP-Tg, 5 ± 3 cells/mm^2, n = 6 for each group; P = 0.68).

Mortality and infarct size do not differ between control and CRP-Tg mice after MI. A total of 86 mice (45 controls and 41 CRP-Tg) underwent surgery for the survival study. Eleven mice (5 controls and 6 CRP-Tg) died of surgical complications: five mice (3 controls and 2 CRP-Tg) died before coronary ligation, three mice (2 controls and 1 CRP-Tg) died after coronary ligation but before extubation, and three mice (0 controls and 3 CRP-Tg) died immediately after extubation. The remaining 75 mice, consisting of 40 controls and 35 CRP-Tg mice, were included in the survival study. Kaplan-Meier analysis revealed that survival 5 wk after MI did not differ between the two groups (Fig. 2*A*). All animals had anterior wall MI at necropsy. LV rupture was found in six control mice and five CRP-Tg mice. Serum CRP levels were 43 ± 17 mg/l in the CRP-Tg mice that were euthanized 5 wk post-MI (n = 14).

We measured infarct sizes at 1 and 5 wk following MI using two approaches: *1*) the ratio of infarct area to total LV area in the LV samples that were cut and opened and *2*) the ratio of infarct lengths to total LV circumferences in the LV cross sections. Infarct size as assessed by either approach was comparable between the two groups (Fig. 2, *D* and *E*). Serum CRP levels were 51 ± 20 mg/l in the CRP-Tg mice that were euthanized 1 wk post-MI (n = 10). In addition, a separate group of animals were euthanized 24 h after MI to assess infarct size by TTC staining. Histological examination showed infarct size to be similar in the two groups (P = 0.85; Fig. 2, *C* and *F*). Infarct size was consistent with our previous data obtained using the same procedure (30). These results indicate that infarct size is not affected by human CRP expression in mice.

CRP-Tg mice have more prominent cardiac hypertrophy and fibrosis in the noninfarcted regions after MI than controls. As shown in Table 1, there was no group difference in body weight 5 wk after MI. The left and right ventricle weight and the left and right ventricle-to-body weight ratio were increased after MI, and these parameters were significantly higher in post-MI CRP-Tg mice than in post-MI controls. The lung weight and the lung-to-body weight ratio were higher in post-MI CRP-Tg mice than in post-MI controls. These data suggest that cardiac hypertrophy and lung congestion associated with MI are more pronounced in CRP-Tg mice.

Histological evaluation revealed the cross-sectional area of cardiac myocytes in the noninfarcted intraventricular septum was increased 5 wk after MI, and the increase in cardiomyo-

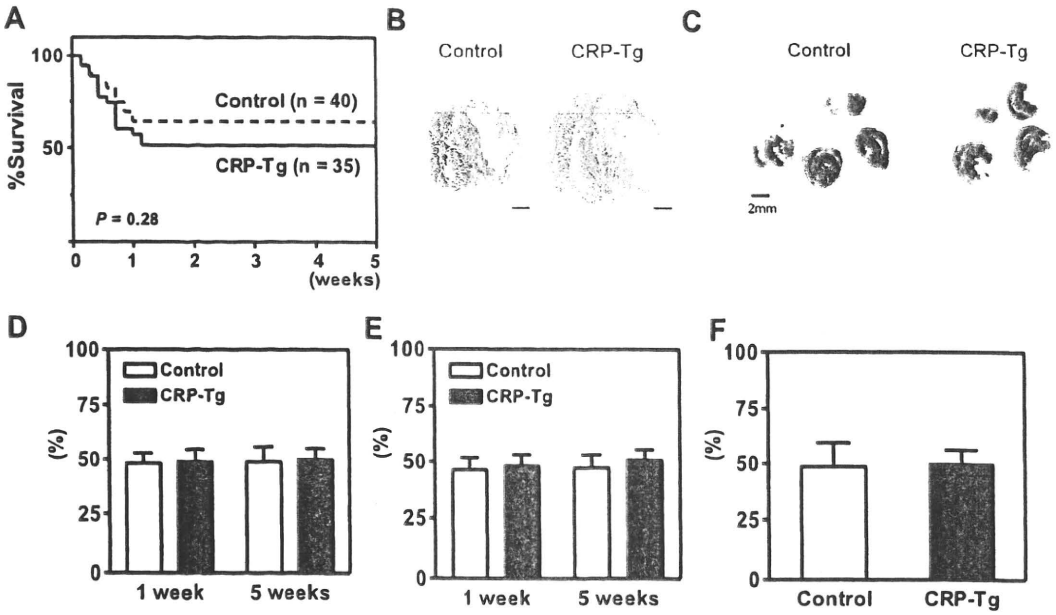

Fig. 2. *A*: seventy-five mice (40 controls and 35 CRP-Tg mice) that recovered from surgery were subjected to the survival study. Kaplan-Meier curve analysis demonstrated that mortality at 5 wk did not differ between the 2 groups (log rank, P = 0.28). *B*: transverse sections of LV at the midventricular level from a control mouse and a CRP-Tg mouse 1 wk after myocardial infarction (MI); Masson's trichrome. *C*: representative pictures of sliced LV cross sections obtained from a control mouse and a CRP-Tg mouse 24 h after MI. Necrotic tissues (white) are distinct from viable tissues (red); 1% triphenyltetrazolium chloride (TTC). *D*: there was no group difference in infarct size 1 and 5 wk after MI as assessed by the ratio of infarct area to total LV area in LV samples. *E*: no group difference in infarct size was found as assessed by the ratio of infarct lengths to total LV circumferences in LV cross sections. *F*: histological examination by TTC staining showed infarct size to be similar in the 2 groups 24 h after MI.

Table 2. *Echocardiographic data of control and CRP-Tg mice before and after MI*

	Pre-MI		Post-MI		
	Control	CRP-Tg	Control	CRP-Tg	ANOVA
n	17	14	17	14	
HR, beats/min	485 ± 56	454 ± 43	492 ± 50	475 ± 53	ns
LVEDD, mm	3.3 ± 0.3	3.2 ± 0.3	5.2 ± 0.5*	5.8 ± 0.4*†	$P < 0.0001$
LVESD, mm	1.7 ± 0.3	1.6 ± 0.3	4.6 ± 0.6*	5.2 ± 0.4*†	$P < 0.0001$
AWth, mm	0.69 ± 0.04	0.69 ± 0.04	0.42 ± 0.07*	0.40 ± 0.05*	$P < 0.0001$
PWth, mm	0.68 ± 0.04	0.68 ± 0.05	0.59 ± 0.08*	0.55 ± 0.08*	$P < 0.0001$
LVEF, %	67 ± 6	67 ± 8	19 ± 5*	13 ± 5*†	$P < 0.0001$

Values are means ± SD; *n*, number of animals studied. HR, heart rate; LVEDD, left ventricular end-diastolic diameter; LVESD, left ventricular end-systolic diameter; AWth, anterior wall thickness; PWth, posterior wall thickness; LVEF, left ventricular ejection fraction. *$P < 0.05$, post-MI vs. pre-MI; †$P < 0.05$, post-MI CRP-Tg vs. post-MI control (Bonferroni's test).

cyte cross-sectional area was greater in CRP-Tg mice than in controls (non-MI control, 270 ± 12 μm^2; non-MI CRP-Tg, 268 ± 16 μm^2; MI control, 389 ± 25 μm^2; MI CRP-Tg, 474 ± 62 μm^2, $n = 6$ for each group; $P < 0.05$ from one-way ANOVA with Bonferroni's test). Staining with Masson's trichrome showed cardiac fibrosis in the noninfarcted intraventricular septum to be enhanced in CRP-Tg mice than in controls 5 wk after MI (control, 0.17 ± 0.05%; CRP-Tg, 0.29 ± 0.07%, $n = 6$ for each group; $P = 0.01$), whereas there was no group difference in percent area of fibrosis in the infarct region (control, 84.8 ± 2.4%; CRP-Tg, 85.6 ± 4.3%, $n = 6$ for each group; $P = 0.68$).

CRP-Tg mice have more LV dilation and worse LV function after MI than controls. Table 2 shows echocardiographic findings before MI and 5 wk after MI. Before MI, there were no differences in heart rate, LV dimensions, wall thickness, or LV function between CRP-Tg and control mice. Five weeks after MI, heart rates did not change. Both anterior and posterior wall thickness decreased to the same extent in both groups. However, LV end-diastolic and end-systolic diameters were larger in CRP-Tg mice, indicating increased chamber dilation. In addition, CRP-Tg mice had lower LV EFs than control mice. To investigate the effects of increased CRP expression on LV remodeling and function at an earlier time point, a different group of animals underwent echocardiography 1 wk after MI. When compared with that of control mice, CRP-Tg mice had larger LV end-diastolic diameter (control, 4.4 ± 0.4 mm, $n = 11$; CRP-Tg, 5.3 ± 0.4 mm, $n = 10$; $P < 0.0001$) and LV end-systolic diameter (control, 3.7 ± 0.5 mm, $n = 11$; CRP-Tg, 4.6 ± 0.4 mm, $n = 10$; $P = 0.0002$) and lower LV EFs (control, 21 ± 5%, $n = 11$; CRP-Tg, 15 ± 4%, $n = 10$; $P = 0.009$). Therefore, the differences in LV size and function between the two groups were already apparent 1 wk after MI. These data suggest that increased CRP expression is associated with more LV dilation and worse LV function after MI.

Hemodynamic measurements were conducted 5 wk after MI. Heart rate, aortic pressure, and LV systolic and end-diastolic pressures did not differ between the CRP-Tg and control groups (Table 3). LV +dP/d*t* was lower in the CRP-Tg group than in the control group ($P = 0.006$). LV −dP/d*t* was also reduced in CRP-Tg mice ($P = 0.002$). These data indicate that increased CRP expression adversely affects LV contractility and relaxation after MI.

Increased apoptosis in the border zones of infarcted hearts from CRP-Tg mice. There were very few TUNEL-positive nuclei in LV sections from uninfarcted mice, and no group difference in the number of TUNEL-positive nuclei was found (control, 12 ± 5 nuclei per 10^5 cells; CRP-Tg, 14 ± 6 nuclei per 10^5 cells, $n = 6$ for each group; $P = 0.46$). This finding indicates that myocardial apoptosis is not induced by human CRP expression in mice under physiological conditions. At 1 wk post-MI, TUNEL-positive nuclei were observed more frequently in the border and infarct zones than in the remote zones in the both groups, which is consistent with our previous findings (30). The rate of myocardial apoptosis in the border zone was higher in the CRP-Tg group than in the control group 1 wk after MI induction (control, 596 ± 275 nuclei per 10^5 cells; CRP-Tg, 1,434 ± 789 nuclei per 10^5 cells, $n = 6$ for each group; $P = 0.03$), whereas the apoptotic rates in the remote and the infarct zones were similar in the two groups (remote: control, 50 ± 12 nuclei per 10^5 cells, and CRP-Tg, 63 ± 24 nuclei per 10^5 cells, $n = 6$ for each group, $P = 0.57$; and infarct: control, 723 ± 314 nuclei per 10^5 cells, and CRP-Tg, 781 ± 435 nuclei per 10^5 cells, $n = 6$ for each group, $P = 0.81$; Fig. 3, *A–C*). We also assessed expression of apoptosis-related genes such as Bcl-2, Bcl-xL, Bax, and Bad in homogenates from the remote, the border, and the infarct zones by real-time RT-PCR ($n = 6$ for each group). Bcl-2 expression in the border zone was decreased by 41% in the CRP-Tg group compared with the control group ($P < 0.05$; Fig. 3*D*). Bcl-2 expression was lower in the infarct zone than in the remote zone, but no group difference in Bcl-2 levels was found in the infarct zone. In contrast, Bax expression in the border zone was increased by 56% in the CRP-Tg group ($P < 0.05$; Fig. 3*E*). Bax expression

Table 3. *Hemodynamic data of control and CRP-Tg mice after MI*

	Control	CRP-Tg
n	10	9
HR, beats/min	402 ± 73	373 ± 75
SBP, mmHg	81 ± 10	76 ± 8
DBP, mmHg	55 ± 9	49 ± 8
LVSP, mmHg	82 ± 11	78 ± 7
LVEDP, mmHg	11 ± 4	13 ± 3
LV +dP/d*t*, mmHg/s	3,788 ± 656	2,974 ± 509*
LV −dP/d*t*, mmHg/s	−2,890 ± 480	−2,230 ± 143*

Values are means ± SD; *n*, number of animals studied. SBP, systolic blood pressure; DBP, diastolic blood pressure; LVSP, left ventricular systolic pressure; LVEDP, left ventricular end-diastolic pressure; LV +dP/d*t*, left ventricular positive change in pressure over time; LV −dP/d*t*, left ventricular negative change in pressure over time. *$P < 0.01$, CRP-Tg vs. control (Student's unpaired *t*-test, 2-tails).

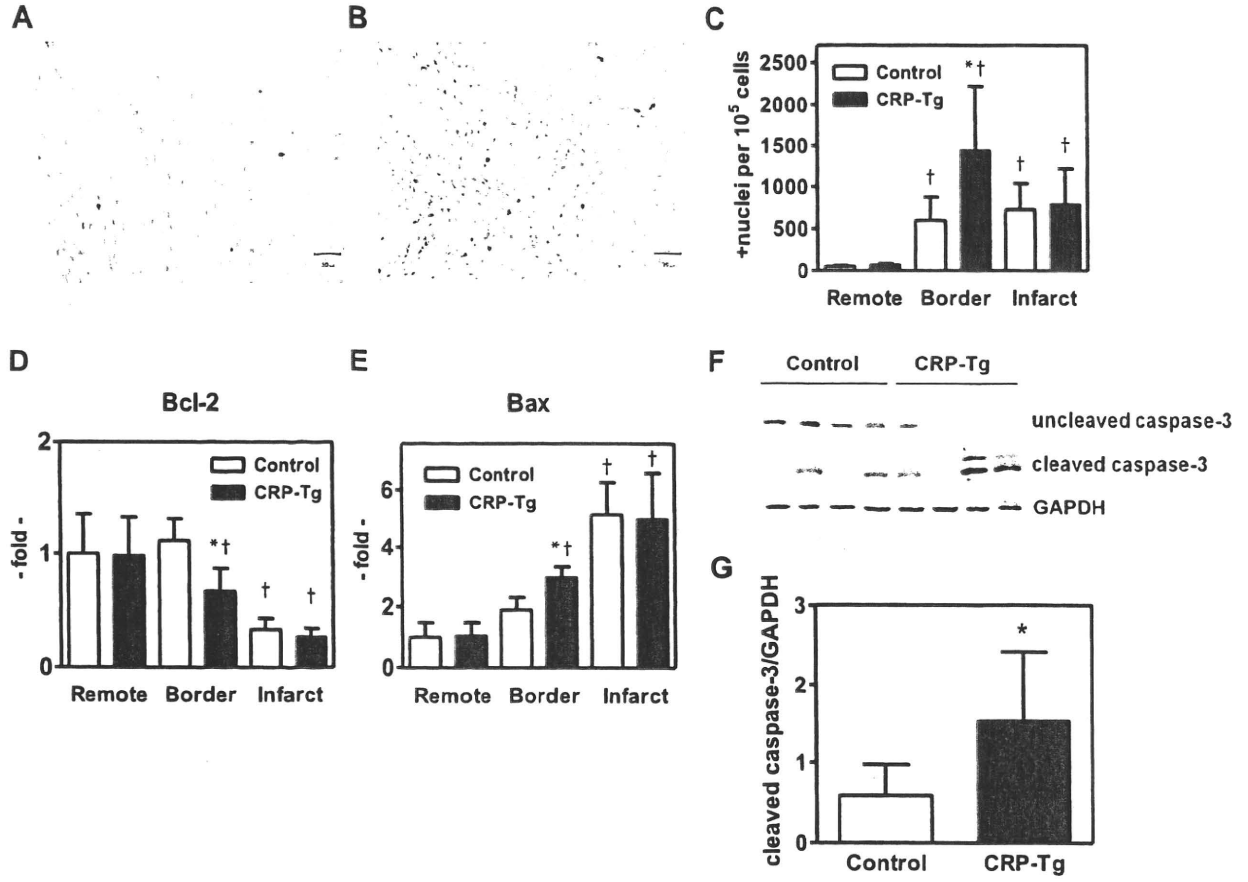

Fig. 3. *A* and *B*: photomicrographs showing blue-stained nuclei (apoptotic) in section of left ventricle from the border zone of a control mouse (*A*) and a CRP-Tg mouse (*B*); TUNEL staining, 400×. *C*: TUNEL-positive nuclei were more frequently observed in the border and the infarct zones than in the remote zones. Apoptotic rate in the border zone was higher in CRP-Tg mice than in control mice 1 wk after MI. *D*: real time RT-PCR showed Bcl-2 expression in the border zone to be lower in CRP-Tg mice than in control mice. Bcl-2 expression was lower in the infarct zone than in the remote zone, but no group difference in Bcl-2 levels was found in the infarct zone. *E*: Bax expression in the border zone was higher in CRP-Tg mice than in control mice. Bax expression was higher in the infarct zone than in the remote zone, but no group difference in Bax levels was found in the infarct zone. Expression of the housekeeping gene GAPDH was used for normalization. *F*: Western blotting of border zone samples for uncleaved caspase-3 and cleaved (active) caspase-3. Increased cleaved caspase-3 content was found in border zone samples from CRP-Tg mice compared with control mice; total caspase-3 was unchanged. *G*: quantification of immunoblotting showed that cleaved caspase-3 expression was higher in border zone samples from CRP-Tg mice compared with control mice. Values are normalized against the corresponding GAPDH levels. Data are means ± SD; $n = 6$ for both groups. *$P < 0.05$, border CRP-Tg vs. border control; †$P < 0.05$, border vs. remote; infarct vs. remote (nonparametric test).

was higher in the infarct zone than in the remote zone, but no group difference in Bax levels was found in the infarct zone. There were no significant group differences in border zone Bcl-xL expression (control, 1.7 ± 0.8 arbitrary unit; CRP-Tg, 1.0 ± 0.4 arbitrary unit; $P = 0.05$) and Bad expression (control, 2.7 ± 0.7 arbitrary unit; CRP-Tg, 4.5 ± 2.1 arbitrary unit; $P = 0.11$). These data suggest that alterations in Bcl-2 and Bax expression are associated with promotion of apoptosis in the border zones of infarcted hearts from CRP-Tg mice. In addition, Western blot analysis showed protein content of cleaved (active form) caspase-3 to be increased in the border zone samples from CRP-Tg mice compared with those from control mice ($P = 0.02$; Fig. 3, *F* and *G*); the sum of uncleaved and cleaved caspase-3 levels was unchanged.

Increased macrophage infiltration, MCP-1 expression, and MMP-9 activity in the border zones of infarcted hearts from CRP-Tg mice. In histological studies, apparent inflammation was seen in the border and the infarct areas but not in the remote region of 1-wk old infarcted hearts. Immunohistochemical studies revealed infiltrating macrophages, as demonstrated by staining with anti-F4/80 antibodies, were predominantly found in the border and the infarct zones. More abundant macrophages (brown stained) were observed in the border zones of infarcted hearts from CRP-Tg mice compared with those from controls ($P = 0.01$; Fig. 4, *A–C*), although the number of macrophages in the infarct zone was comparable between the two groups ($P = 0.30$). The infiltration of neutrophils in the border and the infarct zones, which was a relatively low percentage of infiltrating inflammatory cells at 1 wk post-MI, was similar in the two groups (border: control, 66 ± 18 cells/mm^2, and CRP-Tg, 65 ± 11 cells/mm^2, $P = 0.85$; and infarct: control, 64 ± 10 cells/mm^2, and CRP-Tg 73 ± 10 cells/mm^2, $n = 6$ for each group, $P = 0.43$).

Increased MCP-1 expression in the border zones of infarcted hearts from CRP-Tg mice. Immunohistochemical studies identified macrophages infiltrating in the border and the

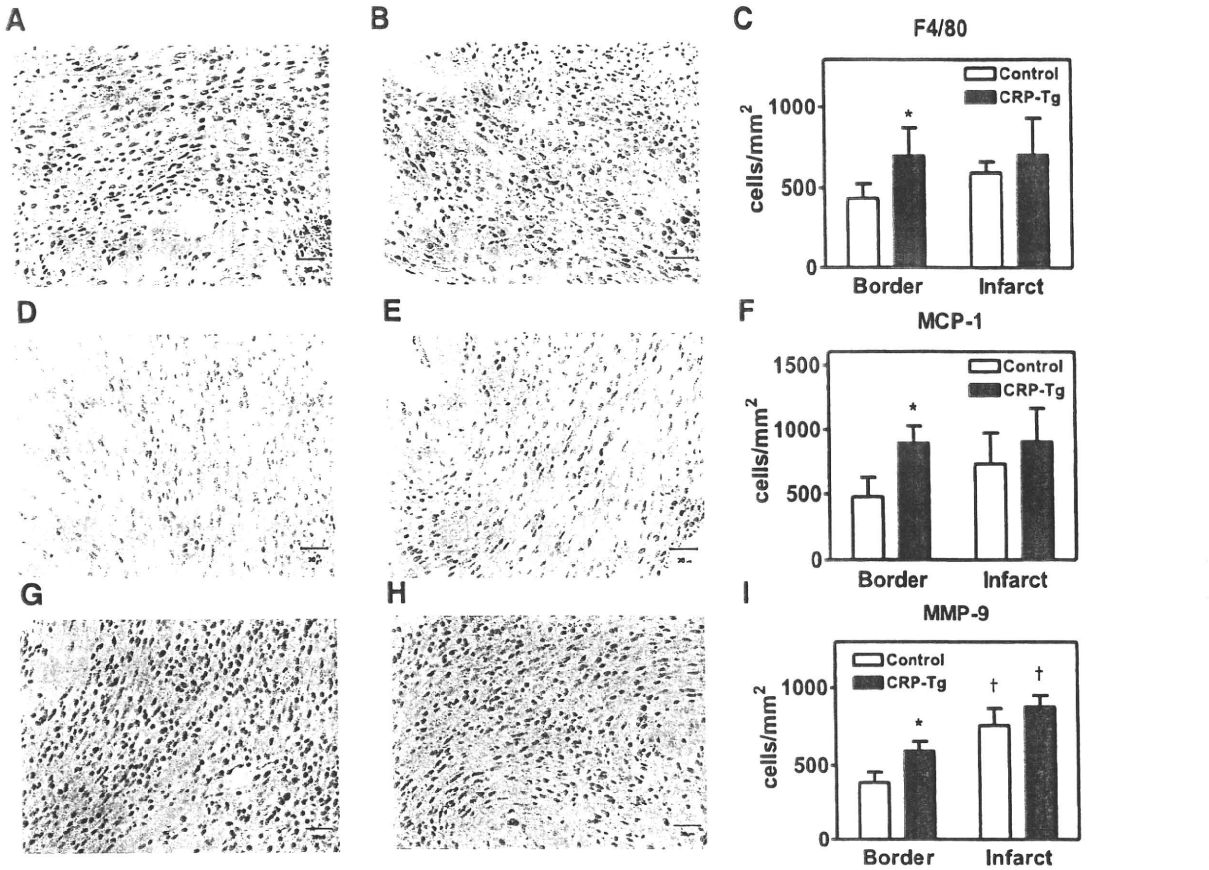

Fig. 4. Immunohistochemical studies stained with antibodies against F4/80 (macrophages), monocyte chemotactic protein (MCP)-1, and matrix metalloproteinase (MMP)-9. *A* and *B*: representative photomicrographs showing brown-stained F4/80 positive cells in a section of the border zone from a control mouse (*A*) and a CRP-Tg mouse (*B*), 400×. *C*: infiltration of F4/80 positive cells was more abundant in the border zones of CRP-Tg mice than in those of control mice 1 wk after MI. *D* and *E*: representative photomicrographs showing brown-stained MCP-1 positive cells in a section of the border zone from a control mouse (*D*) and a CRP-Tg mouse (*E*), 400×. *F*: MCP-1 expression was predominantly found in infiltrating macrophages in the border and infarct zones. More MCP-1 positive cells were seen in the border zones of infarcted hearts from CRP-Tg mice than those from control mice. *G* and *H*: representative photomicrographs showing brown-stained MMP-9 positive cells in a section of the border zone from a control mouse (*G*) and a CRP-Tg mouse (*H*), 400×. *I*: MMP-9 expression was predominantly found in leucocytes and macrophages infiltrating in the border and infarct zones. MMP-9 positive cells were more frequently observed in the infarct zone than in the border zones. More MMP-9 positive cells were seen in the border zones of infarcted hearts from CRP-Tg mice than those from control mice. Data are means ± SD; $n = 6$ for each group. *$P < 0.05$, border CRP-Tg vs. border control; †$P < 0.05$, infarct vs. border (Bonferroni's test).

infarct zones as a main source of MCP-1 (brown stained; Fig. 4, *D* and *E*). More MCP-1 positive cells were seen in the border zones of infarcted hearts from CRP-Tg mice than those from control mice, although there was no group difference in the number of MCP-1 positive cells in the infarct zone (Fig. 4*F*). Western blot analysis also showed MCP-1 protein expression to be increased by 1.5-fold in the border zones, but not in the infarct zone, of infarcted hearts from CRP-Tg mice compared with those from control mice ($P < 0.05$; Fig. 5). MCP-1 expression in remote zone samples was too weak to be detected as clear bands by immunoblotting (data not shown). Serum MCP-1 levels at 1 wk following MI were similar in the two groups (control, 56 ± 24 pg/ml; CRP-Tg, 62 ± 23 pg/ml, $n = 6$ for each group; $P = 0.64$).

Increased MMP-9 activity in the infarct and the border zones of infarcted hearts from CRP-Tg mice. Immunohistochemical studies revealed that MMP-9 expression (brown stained) was predominantly found in leucocytes and macrophages infiltrating in the border and the infarct zones (Fig. 4, *G* and *H*). MMP-9 expression was more frequently observed in the infarct zone than in the border zones. In addition, more MMP-9 positive cells were found in the border zones of infarcted hearts from CRP-Tg mice than those from control mice (Fig. 4*I*). Gelatin zymography showed MMP-9 activity to be higher in border and infarct zones samples from CRP-Tg mice than in those from control mice at 1 wk following MI (Fig. 6, *A–C*). Although MMP-2 activity was enhanced in the border and the infarct zones of infarcted hearts, no group difference in MMP-2 activity was found in either region (Fig. 6*D*).

DISCUSSION

We found that CRP-Tg mice showed greater LV dilation and had poorer LV function with more prominent cardiomyocyte hypertrophy and fibrosis in the viable intraventricular septum after MI than control mice, although survival and infarct size were similar in the two groups. This adverse effect of CRP on LV remodeling was already apparent 1 wk after MI, suggesting a pathogenic role of CRP in the early phase of the post-MI remodeling process. The current study also showed higher

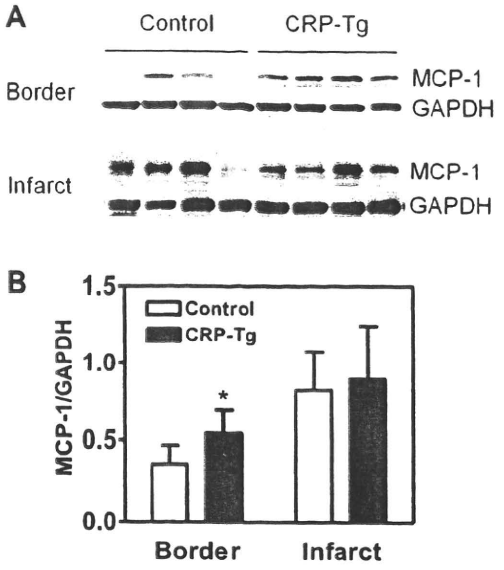

Fig. 5. Western blotting for MCP-1. *A*: increased MCP-1 expression was found in border zone samples from CRP-Tg mice than those from control mice. *B*: quantification of immunoblotting results showed the MCP-1 content to be 1.5-fold higher in border zone samples from CRP-Tg mice than in those from control mice. No group difference was found in infarct zone samples. Values are normalized against the corresponding GAPDH levels. Data are means ± SD; $n = 6$ for each group. $*P < 0.05$, CRP-Tg vs. control (nonparametric test).

apoptotic rates, more macrophage infiltration, and increased MCP-1 expression and MMP-9 activity in the border zones of infarcted hearts from CRP-Tg mice.

CRP is an acute-phase reactant, which responds to various pathological stimuli including infection, inflammation, tissue damage, and neoplasm. Recent experimental studies indicate that CRP per se has multiple biological activities that may be involved in the pathophysiology of various cardiovascular diseases. For instance, CRP induces expressions of adhesion molecules and chemokines such as MCP-1 in in vitro studies (10). CRP reportedly induces apoptosis in human vascular smooth muscle cells as well as rat cardiac myocytes (6, 33). CRP was also reported to attenuate survival, differentiation, and the functions of endothelial progenitor cells (32). CRP-Tg mice that constitutively produce human CRP provide a useful model for studying the biological activities of human CRP in vivo. Some investigators using a crossbreeding method have reported that human CRP expression accelerates the progression of atherosclerosis in apoE-deficient mice (22, 26), although conflicting data have been presented by other laboratories (12, 14, 31).

In acute MI, CRP peaks at 2 to 3 days after the onset, and the peak level is a strong predictor of adverse clinical outcomes (2, 3, 29). Although the pathogenic importance of CRP remains undetermined in the acute MI setting, CRP colocalizes with activated complement in human infarcted tissues (15). Griselli et al. (9) reported that injection of human CRP after coronary artery occlusion increases infarct size in rats. In the present study, however, increased CRP expression did not affect infarct size in our transgenic mouse model. This difference may be explained by the different species (mouse vs. rat) used, the different experimental conditions (transgene expression vs. protein injection), and the extent of infarct size. The average infarct size was ~50% in our study, whereas it was 17% for the vehicle-treated group and 25% for the CRP-treated group in their study (9). It is noteworthy that, in our study, increased CRP expression was associated with more LV dilation and worse LV function after MI without altering infarct size. To our knowledge, no study has shown direct in vivo effects of CRP on the development of adverse LV remodeling after MI. We therefore asked how increased CRP expression could modulate the post-MI inflammatory response and healing process as well as apoptosis, which might be responsible for deterioration of cardiac remodeling after MI in our CRP-Tg mice.

The post-MI inflammatory response plays a critical role in the pathophysiology of infarct expansion and LV remodeling (8). We previously reported post-MI peripheral monocytosis to be associated with LV dysfunction and LV aneurysm (17) and that granulocyte-macrophage colony-stimulating factor induction in a rat MI model resulted in exaggerated LV remodeling

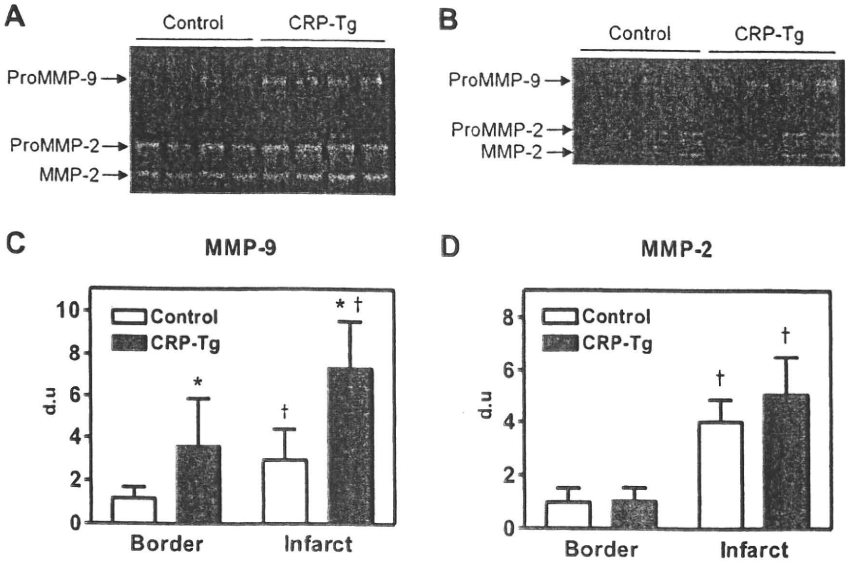

Fig. 6. *A* and *B*: gelatin zymography for MMP activities in infarct zone samples (*A*) and border zone samples (*B*). *C*: MMP-9 activity in the border and the infarct zones was increased in CRP-Tg mice 1 wk after MI. *D*: although MMP-2 activity was enhanced in the border and the infarct zones of infarcted hearts, no group difference in MMP-2 activity was found in either region. Data are means ± SD; $n = 6$ for each group. $*P < 0.05$, border CRP-Tg vs. border control; $\dagger P < 0.05$, infarct vs. border (nonparametric test). du, Densitometric unit.

with increased infiltration of monocyte-derived macrophages and dendritic cells and impaired reparative fibrosis in the infarcted area (18, 20). In the present study, immunohistochemical studies have shown more pronounced macrophage infiltration in the border zones of infarcted hearts from CRP-Tg mice than in those from control mice. In addition, MCP-1 expression was predominantly found in infiltrating macrophages. Western blot analysis also showed MCP-1 expression in the border zones to be increased in CRP-Tg mice. These results indicate that increased CRP expression intensifies the inflammatory response after MI through local macrophage infiltration and activation, although the precise mechanisms by which CRP enhances this infiltration and activation in the present context remain uncertain. A recent clinical study with endomyocardial biopsies has shown the evidence for colocalization of CRP with complements and macrophages in the myocardium of patients with dilated cardiomyopathy (34). Since CRP is reported to upregulate MCP-1-mediated chemotaxis in human monocytes (10), CRP might be directly involved in increased macrophage infiltration and activation around the necrotic tissues.

Myocardial apoptosis is one of the key factors contributing to the progression of LV remodeling and heart failure after MI (21, 25). Moreover, apoptosis of cardiac myocytes is reported to peak during the first several days following MI in the ischemic area (5, 16), which is consistent with our previous data showing that myocardial apoptosis frequently occurs in the infarct border zone in the early phase after MI (30). In the present study, apoptotic rates were higher in the border zones of infarcted hearts from CRP-Tg mice compared with those from control mice, where proapoptotic gene expression profiles were noted. One report showed that CRP induces ischemia-related apoptosis of cardiac myocytes in vitro (33). Thus increased CRP expression may promote the development of LV remodeling after MI through increased apoptosis in the border zone.

MMPs, major regulators of extracellular matrix degradation, have been shown to be involved in the pathogenesis of LV remodeling after MI. Several studies in genetically manipulated mice documented that gelatinases such as MMP-2 and MMP-9 play a critical role in the remodeling process and contributing to LV rupture (11, 19). MMP-9 is predominately found in leukocytes and macrophages in infarcted regions and targeted deletion of MMP-9 prevents LV rupture in the acute MI setting (11). In the present study, more infiltrating macrophages with increased MMP-9 expression were seen in the border zones of infarcted hearts from CRP-Tg mice compared with those from control mice. Moreover, MMP zymography showed increased MMP-9 activity in the border and the infarct zones of infarcted hearts from CRP-Tg mice. Abe et al. (1) have demonstrated that CRP increases gene expression and activity of MMP-9 in human macrophages, suggesting a direct effect of CRP on MMP-9 activity in macrophages. Thus increased MMP-9 activity in association with macrophages infiltration in CRP-Tg mice may impair the healing process after MI, resulting in adverse LV remodeling.

The current study provides the first evidence for the direct in vivo effect of human CRP on the post-MI remodeling process in an animal model. Although there is considerable variability among species with respect to the biological and pathological functions of CRP, one would assume that CRP partially involves in the pathogenesis of the post-MI remodeling process in human hearts. Further studies are needed to confirm this deleterious effect of CRP on adverse LV remodeling in a clinical post-MI setting.

In conclusion, increased human CRP expression exacerbates LV dysfunction and adverse LV remodeling after MI without affecting infarct size in mice.

ACKNOWLEDGMENTS

We thank Shigeyuki Kasai (Oriental Yeast) and Tomomichi Kanabayashi (Biopathology Institute) for technical assistance.

GRANTS

This work was partly supported by the Medical School Faculty and Alumni Grant from Keio University Medical Science Fund (to T. Anzai) and the Keio Gijuku Academic Development Fund (to T. Takahashi) and the Global Center of Excellence (G-COE) at Keio University (to H. Kaneko).

DISCLOSURES

No conflicts of interest, financial or otherwise, are declared by the author(s).

REFERENCES

1. **Abe N, Osanai T, Fujiwara T, Kameda K, Matsunaga T, Okumura K.** C-reactive protein-induced upregulation of extracellular matrix metalloproteinase inducer in macrophages: inhibitory effect of fluvastatin. *Life Sci* 146: 287–298, 2006.
2. **Anzai T, Yoshikawa T, Kaneko H, Maekawa Y, Iwanaga S, Asakura Y, Ogawa S.** Association between serum C-reactive protein elevation and left ventricular thrombus formation after first anterior myocardial infarction. *Chest* 125: 384–389, 2004.
3. **Anzai T, Yoshikawa T, Shiraki H, Asakura Y, Akaishi M, Mitamura H, Ogawa S.** C-reactive protein as a predictor of infarct expansion and cardiac rupture after a first Q-wave acute myocardial infarction. *Circulation* 96: 778–784, 1997.
4. **Bayat H, Swaney JS, Ander AN, Dalton N, Kennedy BP, Hammond HK, Roth DM.** Progressive heart failure after myocardial infarction in mice. *Basic Res Cardiol* 97: 206–213, 2002.
5. **Bialik S, Geenen DL, Sasson IE, Cheng R, Horner JW, Evans SM, Lord EM, Koch CJ, Kitsis RN.** Myocyte apoptosis during acute myocardial infarction in the mouse localizes to hypoxic regions but occurs independently of p53. *J Clin Invest* 100: 1363–1372, 1997.
6. **Blaschke F, Bruemmer D, Yin F, Takata Y, Wang W, Fishbein MC, Okura T, Higaki J, Graf K, Fleck E, Hsueh WA, Law RE.** C-reactive protein induces apoptosis in human coronary vascular smooth muscle cells. *Circulation* 110: 579–587, 2004.
7. **Danenberg HD, Szalai AJ, Swaminathan RV, Peng L, Chen Z, Seifert P, Fay WP, Simon DI, Edelman ER.** Increased thrombosis after arterial injury in human C-reactive protein-transgenic mice. *Circulation* 108: 512–515, 2003.
8. **Frantz S, Bauersachs J, Ertl G.** Post-infarct remodelling: contribution of wound healing and inflammation. *Cardiovasc Res* 81: 474–481, 2009.
9. **Griselli M, Herbert J, Hutchinson WL, Taylor KM, Sohail M, Krausz T, Pepys MB.** C-reactive protein and complement are important mediators of tissue damage in acute myocardial infarction. *J Exp Med* 190: 1733–1740, 1999.
10. **Han KH, Hong KH, Park JH, Ko J, Kang DH, Choi KJ, Hong MK, Park SW, Park SJ.** C-reactive protein promotes monocyte chemoattractant protein-1-mediated chemotaxis through upregulation CC chemokine receptor 2 expression in human monocytes. *Circulation* 109: 2566–2571, 2004.
11. **Heymans S, Luttun A, Nuyens D, Theilmeier G, Creemers E, Moons L, Dyspersin GD, Cleutjens JP, Shipley M, Angellilo A, Levi M, Nübe O, Baker A, Keshet E, Lupu F, Herbert JM, Smits JF, Shapiro SD, Baes M, Borgers M, Collen D, Daemen MJ, Carmeliet P.** Inhibition of plasminogen activators or matrix metalloproteinases prevents cardiac rupture but impairs therapeutic angiogenesis and causes cardiac failure. *Nat Med* 10: 1135–1142, 1999.
12. **Hirschfield GM, Gallimore JR, Kahan MC, Hutchinson WL, Sabin CA, Benson GM, Dhillon AP, Tennent GA, Pepys MB.** Transgenic

human C-reactive protein is not proatherogenic in apolipoprotein E-deficient mice. *Proc Natl Acad Sci USA* 102: 8309–8314, 2005.

13. **Katada J, Meguro T, Saito H, Ohashi A, Anzai T, Ogawa S, Yoshikawa T.** Persistent cardiac aldosterone synthesis in angiotensin II type 1A receptor-knockout mice after myocardial infarction. *Circulation* 111: 2157–2164, 2005.
14. **Kovacs A, Tornvall P, Nilsson R, Tegnér J, Hamsten A, Björkegren J.** Human C-reactive protein slows atherosclerosis development in a mouse model with human-like hypercholesterolemia. *Proc Natl Acad Sci USA* 104: 13768–13773, 2007.
15. **Lagrand WK, Niessen HW, Wolbink GJ, Jaspars LH, Visser CA, Verheugt FW, Meijer CJ, Hack CE.** C-reactive protein colocalizes with complement in human hearts during acute myocardial infarction. *Circulation* 95: 97–103, 1997.
16. **Li Q, Li B, Wang X, Leri A, Jana KP, Liu Y, Kajstura J, Baserga R, Anversa P.** Overexpression of insulin-like growth factor-1 in mice protects from myocyte death after infarction, attenuating ventricular dilation, wall stress, and cardiac hypertrophy. *J Clin Invest* 100: 1991–1999, 1997.
17. **Maekawa Y, Anzai T, Yoshikawa T, Asakura Y, Takahashi T, Ishikawa S, Satoh T, Mitamura H, Ogawa S.** Prognostic significance of peripheral monocytosis after reperfused acute myocardial infarction: a possible role for left ventricular remodeling. *J Am Coll Cardiol* 39: 241–246, 2002.
18. **Maekawa Y, Anzai T, Yoshikawa T, Sugano Y, Mahara K, Kohno T, Takahashi T, Ogawa S.** Effect of granulocyte-macrophage colony-stimulating factor inducer on left ventricular remodeling after acute myocardial infarction. *J Am Coll Cardiol* 44: 1510–1520, 2004.
19. **Matsumura S, Iwanaga S, Mochizuki S, Okamoto H, Ogawa S, Okada Y.** Targeted deletion or pharmacological inhibition of MMP-2 prevents cardiac rupture after myocardial infarction in mice. *J Clin Invest* 115: 599–609, 2005.
20. **Naito K, Anzai T, Sugano Y, Maekawa Y, Kohno T, Yoshikawa T, Matsuno K, Ogawa S.** Differential effects of GM-CSF and G-CSF on infiltration of dendritic cells during early left ventricular remodeling after myocardial infarction. *J Immunol* 181: 5691–5701, 2008.
21. **Palojoki E, Saraste A, Eriksson A, Pulkki K, Kallajoki M, Voipio-Pulkki LM, Tikkanen I.** Cardiomyocyte apoptosis and ventricular remodeling after myocardial infarction in rats. *Am J Physiol Heart Circ Physiol* 280: H2726–H2731, 2001.
22. **Paul A, Ko KWS, Li L, Yechoor V, McCrory MA, Szalai AJ, Chan L.** C-reactive protein accelerates the progression of atherosclerosis in apolipoprotein E-deficient mice. *Circulation* 109: 647–655, 2004.
23. **Ridker PM, Cushman M, Stampfer MJ, Tracy RP, Hennekens CH.** Inflammation, aspirin, and the risk of cardiovascular disease in apparently healthy men. *N Engl J Med* 336: 973–979, 1997.
24. **Ridker PM, Rifai N, Rose L, Buring JE, Cook NR.** Comparison of C-reactive protein and low-density lipoprotein cholesterol levels in the prediction of first cardiovascular events. *N Engl J Med* 347: 1557–1565, 2002.
25. **Sam F, Sawyer DB, Chang DL, Eberli FR, Ngoy S, Jain M, Amin J, Apstein CS, Colucci WS.** Progressive left ventricular remodeling and apoptosis late after myocardial infarction in mouse heart. *Am J Physiol Heart Circ Physiol* 279: H422–H428, 2000.
26. **Schwedler SB, Amann K, Wernicke K, Krebs A, Nauck M, Wanner C, Potempa LA, Galle J.** Native C-reactive protein increases whereas modified C-reactive protein reduces atherosclerosis in apolipoprotein E-knockout mice. *Circulation* 112: 1016–1023, 2005.
27. **Sugano Y, Anzai T, Yoshikawa T, Maekawa Y, Kohno T, Mahara K, Naito K, Ogawa S.** Granulocyte colony-stimulating factor attenuates early ventricular expansion after experimental myocardial infarction. *Cardiovasc Res* 65: 446–456, 2005.
28. **Suleiman M, Khatib R, Agmon Y, Mahamid R, Boulos M, Kapeliovich M, Levy Y, Beyar R, Markiewicz W, Hammerman H, Aronson D.** Early inflammation and risk of long-term development of heart failure and mortality in survivors of acute myocardial infarction: predictive role of C-reactive protein. *J Am Coll Cardiol* 47: 962–968, 2006.
29. **Takahashi T, Anzai T, Yoshikawa T, Maekawa Y, Asakura Y, Satoh T, Mitamura H, Ogawa S.** Serum C-reactive protein elevation in left ventricular remodeling after acute myocardial infarction–role of neurohormones and cytokines. *Int J Cardiol* 88: 257–265, 2003.
30. **Takahashi T, Tang T, Lai NC, Roth DM, Rebolledo B, Saito M, Lew WYW, Clopton P, Hammond HK.** Increased cardiac adenylyl cyclase expression is associated with increased survival after myocardial infarction. *Circulation* 114: 388–396, 2006.
31. **Trion A, de Maat MP, Jukema JW, van der Laarse A, Maas MC, Offerman EH, Havekes LM, Szalai AJ, Princen HM, Emeis JJ.** No effect of C-reactive protein on early atherosclerosis development in apolipoprotein E*3-Leiden/human C-reactive protein transgenic mice. *Arterioscler Thromb Vasc Biol* 25: 1635–1640, 2005.
32. **Verma S, Kuliszewski MA, Li SH, Szmitko PE, Zucco L, Wang CH, Badiwala MV, Mickle DA, Weisel RD, Fedak PW, Stewart DJ, Kutryk MJ.** C-reactive protein attenuates endothelial progenitor cell survival, differentiation, and function: further evidence of a mechanistic link between C-reactive protein and cardiovascular disease. *Circulation* 109: 2058–2067, 2004.
33. **Yang J, Wang J, Zhu S, Chen X, Wu H, Yang D, Zhang J.** C-reactive protein augments hypoxia-induced apoptosis through mitochondrion-dependent pathway in cardiac myocytes. *Mol Cell Biochem* 310: 215–226, 2008.
34. **Zimmermann O, Bienek-Ziolkowski M, Wolf B, Vetter M, Baur R, Mailänder V, Hombach V, Torzewski J.** Myocardial inflammation and non-ischaemic heart failure: is there a role for C-reactive protein? *Basic Res Cardiol* 104: 591–599, 2009.

Journal of Molecular and Cellular Cardiology 50 (2011) 117–127

Contents lists available at ScienceDirect

Journal of Molecular and Cellular Cardiology

journal homepage: www.elsevier.com/locate/yjmcc

Original article

Impact of long-term caloric restriction on cardiac senescence: Caloric restriction ameliorates cardiac diastolic dysfunction associated with aging

Ken Shinmura [a,*], Kayoko Tamaki [a], Motoaki Sano [b,c], Mitsushige Murata [b], Hiroyuki Yamakawa [b], Hideyuki Ishida [d], Keiichi Fukuda [b]

[a] Division of Geriatric Medicine, Department of Internal Medicine, Keio University School of Medicine, Tokyo, 160-8582, Japan
[b] Division of Cardiology, Department of Internal Medicine, Keio University School of Medicine, Tokyo, 160-8582, Japan
[c] Precursory Research for Embryonic Science and Technology (PRESTO), Japan Science and Technology Agency, Saitama, 332-0012, Japan
[d] Department of Physiology, Tokai University School of Medicine, Isehara, 259-1193, Japan

ARTICLE INFO

Article history:
Received 2 June 2010
Received in revised form 5 October 2010
Accepted 17 October 2010
Available online 23 October 2010

Keywords:
Aging
Autophagy
Calcium
Cardiac function
Nutrition
Sarcoplasmic reticulum

ABSTRACT

Approximately half of older patients with congestive heart failure have normal left ventricular (LV) systolic but abnormal LV diastolic function. In mammalian hearts, aging is associated with LV diastolic dysfunction. Caloric restriction (CR) is expected to retard cellular senescence and to attenuate the physiological decline in organ function. Therefore, the aim of the present study was to investigate the impact of long-term CR on cardiac senescence, in particular the effect of CR on LV diastolic dysfunction associated with aging. Male 8-month-old Fischer344 rats were divided into ad libitum fed and CR (40% energy reduction) groups. LV function was evaluated by echocardiography and cardiac senescence was compared between the two groups at the age of 30-month-old. (1) Echocardiography showed similar LV systolic function, but better LV diastolic function in the CR group. (2) Histological analysis revealed that CR attenuated the accumulation of senescence-associated β-galactosidase and lipofuscin and reduced myocyte apoptosis. (3) In measurements of $[Ca^{2+}]_i$ transients, the time to 50% relaxation was significantly smaller in the CR group, whereas F/F_0 was similar. (4) CR attenuated the decrease in sarcoplasmic reticulum calcium ATPase 2 protein with aging. (5) CR suppressed the mammalian target of rapamycin (mTOR) pathway and increased the ratio of conjugated to cytosolic light chain 3, suggesting that autophagy is enhanced in the CR hearts. In conclusion, CR improves diastolic function in the senescent myocardium by amelioration of the age-associated deterioration in intracellular Ca^{2+} handling. Enhanced autophagy via the suppression of mTOR during CR may retard cardiac senescence.

1. Introduction

The clinical problem of congestive heart failure (CHF) is increasing in developed countries confronted with an aging society [1,2]. The morbidity of CHF increases with aging, as does mortality. Interestingly, approximately half of older patients with CHF show normal LV systolic but abnormal LV diastolic function. Recent studies have revealed that the prognosis of CHF associated with LV diastolic dysfunction is similar to that associated with LV systolic dysfunction [3]. However, therapeutic strategies aimed at improving LV diastolic dysfunction have not been established. In mammalian hearts, aging is associated with impaired cardiac relaxation [4–6]. Senescent cardiomyocytes are characterized by prolonged relaxation, diminished contraction velocity, a decrease in β-adrenergic response, and increased myocardial stiffness. This impairment in diastolic function contributes, in part, to the increased incidence of CHF in the elderly [2].

Caloric restriction (CR) is the established intervention for which anti-aging effects have been proven scientifically [7,8]. CR can retard cellular senescence and attenuate the physiological decline in organ function. Hearts become more susceptible to various stresses with aging [5,6,9]. We have demonstrated that short-term (4 weeks) and prolonged (6 months) CR confers cardioprotection in aged and middle-aged rats, respectively [9,10]. These results indicate that CR retards cardiac senescence from the aspect of myocardial ischemic tolerance.

In addition, recent clinical studies have demonstrated that CR, when accompanied by significant body weight loss, has cardiac-specific effects that ameliorate LV diastolic function in healthy subjects [11,12], as well as in patients with type 2 diabetes mellitus (T2DM) [13]. Thus, clinical application of CR and the development of CR mimetics that can replicate the effects of CR have considerable potential as novel therapeutic approaches for the treatment of

* Corresponding author. Division of Geriatric Medicine, Department of Internal Medicine, Keio University School of Medicine, 35 Shinanomachi, Shinjuku-ku, Tokyo, Japan 160-8582. Tel.: +81 3 3353 1211x62915; fax: +81 3 5269 2468.
E-mail address: shimmura@sc.itc.keio.ac.jp (K. Shinmura).

0022-2828/$ – see front matter © 2010 Elsevier Ltd. All rights reserved.
doi:10.1016/j.yjmcc.2010.10.018

patients with diastolic dysfunction. However, the exact mechanism(s) by which CR improves cardiac diastolic dysfunction remains unknown. Furthermore, how long-term CR modulates cardiac senescence has not been fully evaluated.

Therefore, the aim of the present study was to investigate the impact of long-term CR, which started at the age of 8-month-old and continued till the age of 30-month-old, on cardiac senescence, in particular the effects of CR on cardiac diastolic dysfunction associated with aging. Our results strongly suggest that long-term CR improves diastolic function in the senescent myocardium by ameliorating the age-associated deterioration in myocyte relaxation. Furthermore, our results indicate that attenuation of the decrease in sarcoplasmic reticulum calcium ATPase (SERCA) 2 with aging and enhanced autophagic flux are associated with functional improvements in the aged heart.

2. Materials and methods

All procedures in the present study conformed to the principles outlined in the *Guide for the Care and Use of Laboratory Animals* published by the US National Institutes of Health (NIH Publication No. 85-23, revised 1996) and were approved by the Institutional Animal Care and Use Committee of Keio University School of Medicine.

2.1. CR protocols

Seven-month-old male Fischer344 rats were obtained from Charles-River Japan. Rats were housed in individual cages according to institutional protocols at Keio University Experimental Animal Centre and fed ad libitum for 2 weeks with a modified semipurified diet A (Oriental Yeast Co.) (Supplemental Table 1). The average caloric intake was calculated from daily food intake over this 2-week period. After weaning, rats at the age of 8-month-old were randomly divided into two groups: AL rats ($n = 24$) continued to be fed ad libitum with control diet A, whereas CR rats ($n = 20$) were fed first with 90% of the average caloric intake during the 2-week run-in period (10% restriction), followed by 60% of the average caloric intake (40% energy reduction) till the age of 30-month-old using modified semipurified diets B and C. Modified semipurified diets B and C comprised the same calorie per weight, but were enriched in vitamins and minerals by 11% and 67%, respectively, compared with diet A (Supplemental Table 1). We reduced the daily calorie intake by decreasing food weight to 90% and 60% in the modified semipurified diets B and C, respectively. Three-month-old rats were used as the young controls (YC).

2.2. Echocardiography

At the age of 29-month-old, rats were anesthetized with 1.5% isoflurane inhalation and were anchored to a positionable platform in the supine position. Short axis echocardiography and Doppler echocardiographic measurements from the apical 4-chamber view were performed using the Vevo2100 echocardiography (VisualSonics). To obtain tissue Doppler imaging (TDI), sample volume was placed at the septal side of the mitral annulus and early (E′) and late (A′) diastolic mitral annular velocities were measured.

2.3. Histological examination

Senescence-associated β-galactosidase and lipofuscin were assessed in fresh frozen tissue sections. Briefly, cryostat sections were fixed in 3% formaldehyde and washed in phosphate-buffered saline (PBS) at room temperature. Slides were immersed in freshly prepared β-galactosidase staining solution [1 mg/mL X-gal in dimethylformamide, 40 mM citric acid, sodium phosphate (pH 6.0), 5 mM potassium ferrocyanide, 5 mM potassium ferricyanide, 150 mM NaCl, and 2 mM $MgCl_2$] and incubated at 37 °C overnight. Stained slides were washed with PBS and counterstained with nuclear fast red. Other frozen tissue sections were fixed with 3% formaldehyde and viewed immediately by fluorescence microscopy with a 590 nm filter to assess autofluorescence of the myocardium [14]. Apoptotic cardiomyocytes were assessed using the ApopTag In Situ Apoptosis Detection Kit (Serologicals). Tissue sections were also stained with 4′,6-diamidino-2-phenylindole (DAPI) to visualize nuclei. Percentage of TUNEL-positive myocytes was calculated by counting 10,000 nuclei in each group. Part of the heart was fixed overnight in 10% formalin at 4 °C, dehydrated with 70% ethanol, mounted in paraffin, and sectioned (5 μm). Sections were stained with Hematoxylin and Eosin, Masson's trichrome, and Picrosirius red (for fibrosis). The proportion of the fibrotic area was determined in slides stained with Picrosirius red using a BIOREVO fluorescence microscope (BZ-9000, Keyence).

2.4. Lipofuscin assay

Heart tissue was ground in liquid nitrogen and homogenized in chloroform–methanol (1:20, w:v). After centrifugation, the chloroform-rich layer was mixed with the methanol. The fluorescence in this fraction was measured at an excitation wavelength of 350 nm and emission wavelength of 485 nm using a spectrofluorimeter [15]. Fluorescence intensity at 485 nm was expressed as units/100 mg tissue.

2.5. Isolation of cardiomyocytes

Ventricular cardiomyocytes were isolated from AL and CR rats as described previously [16] ($n = 6$, each). Briefly, hearts were mounted on a Langendorff apparatus and perfused with Tyrode solution containing 0.1 mM Ca^{2+}. Type II collagenase (Worthington) was then added to the perfusate. After 30 min, the hearts were taken down, ventricles minced, and myocytes dissociated by trituration. Subsequently, myocytes were filtered, centrifuged, and resuspended in MEM containing 1 mM Ca^{2+}. Myocytes were used within 6 h of isolation.

2.6. Measurement of $[Ca^{2+}]_i$

Myocytes were loaded at 22 °C with Fluo-4 AM (10 μM; Molecular Probes) for 30 min, washed out, and then allowed to sit for a further 30 min to allow for intracellular deesterification. The cell fluorescence measurement was performed at room temperature using a Zeiss LSM-510 confocal microscope (5-Live mode). Laser excitation (488 nm) and emission (543 nm) were used for detecting Fluo-4 fluorescent signal [17]. Myocytes were incubated with 1.0 mM Ca^{2+} Tyrode solution and stimulated via platinum electrodes connected to a stimulator at a frequency of 1 Hz. Contraction amplitude and rates of contraction and relaxation were recorded online with a video edge-detection system and data acquisition software as described previously [17]. SR Ca^{2+} content was evaluated after rapid application of caffeine (10 mM) [18] and expressed as relative value of baseline F/F_0.

2.7. SERCA activity

SERCA activity was assayed based on a pyruvate/NADH coupled reaction as described previously [19]. Oxidation of NADH was assessed at 37 °C in the membranous fractions from heart homogenate according to the difference between the total absorbance and basal absorbance at a wavelength of 340 nm. SERCA activity was expressed as nmol ATP/mg protein/min.

2.8. Western blotting

Total protein was extracted from frozen hearts. Equal amounts of total proteins (20–40 μg) were subjected to SDS-PAGE [9,10]. The primary antibodies used in the present study were anti-SERCA2, anti-phospholamban (PLB) (Affinity BioReagents), anti-phosphorylated PLB (Ser^{16}) (ThermoScientific), anti-Na^+–Ca^{2+} exchanger (NCX) 1 (Abcam), anti-troponin I, anti-phosphorylated troponin I ($Ser^{23/24}$), anti-Beclin1, anti-mammalian target of rapamycin (mTOR), anti-phosphorylated mTOR (Ser^{2448}), anti-p70 S6 kinase (S6K), anti-phosphorylated S6K (Thr^{389}) (Cell Signaling Technology), anti-$p16^{INK4a}$ (Santa Cruz Biotechnology), anti-light chain (LC) 3 (Medical & Biological Laboratories), and anti-glyceraldehydes 3-phosphate dehydrogenase (GAPDH) (Chemicon International). To assess protein carbonyls, protein extracts were reacted with 2,4-dinitrophenylhydrazine (DNPH) using the Oxyblot kit (Millipore) with a modification as described previously [20].

2.9. Chloroquine treatment

We evaluated the effect of chloroquine, a lysosomal protease inhibitor, on the expression of LC3-II using male 20-month-old rats fed with either AL or CR for 12 months. Alzet osmotic pump was implanted subcutaneously in the infrascapular region of either AL or CR rat. Chloroquine (10 mg/kg per day; Sigma) or saline vehicle was continuously administered for 4 weeks [14]. Three hearts from each group were used for Western immunoblotting.

2.10. Statistical analysis

Data are presented as the mean ± SEM. For intergroup comparisons, data were analyzed by one-way ANOVA, followed by Student's t tests for unpaired data with Bonferroni's correction. $P<0.05$ was considered significant.

3. Results

3.1. Mortality

During the 22-month observation period, thirteen out of 24 rats in the AL group and 5 out of 20 rats in the CR group died. Thus, as expected, mortality was significantly less in the CR group than in the AL group ($P<0.05$, Supplemental Fig. 1).

3.2. Echocardiographic findings

Aged hearts in the AL group exhibited an increase in LV mass and slightly reduced LV systolic parameters (Table 1). Although the E/A ratio was significantly higher in the AL group than that in the YC group, the deceleration time of the E wave and isovolumic relaxation time were longer in the AL group. In addition, TDI showed a remarkable decrease in peak E′ velocity, a modest decrease in peak A′ velocity, and a subsequent decrease in the E′/A′ ratio in the AL group. These results indicate that LV diastolic function was severely impaired in aged hearts.

Echocardiographic parameters of LV systolic function were similar between AL and CR hearts (Table 1). CR attenuated the increase in LV mass with aging. As expected, long-term CR preserved LV diastolic function. The E/A ratio was similar between AL and CR hearts, but the deceleration time of the E wave and isovolumic relaxation time were significantly shorter in the CR group. TDI showed a higher E′ velocity and a greater E′/A′ ratio in the CR group.

3.3. Body weight and ventricular weight

Since rats were randomly divided into two groups, there was no difference in body weight (BW) at the age of 8-month-old between AL and CR [AL: 355 ± 5 (n = 16) vs. CR: 356 ± 8 (n = 14) g; n.s.]. BW at the age of 30-month-old was significantly heavier in the AL group than that in the CR group [AL: 348 ± 5 (n = 8) vs. CR: 290 ± 4 (n = 10) g; $P<0.05$]. The ventricular weight was also heavier in the AL group [AL: 1.16 ± 0.02 (n = 8) vs. CR: 0.95 ± 0.02 (n = 10) g; $P<0.05$], but the ratio of ventricular weight to BW was similar between AL and CR [AL: 0.326 ± 0.009 (n = 8) vs. CR: 0.329 ± 0.006 (n = 10) %; n.s.].

Table 1
Echocardiographic parameters.

	YC	AL	CR
LV mass (mg)	587 ± 19 (n = 5)	691 ± 21$^+$ (n = 8)	616 ± 12* (n = 10)
Ejection fraction (%)	76.8 ± 2.2 (n = 5)	71.4 ± 1.7$^+$ (n = 8)	69.8 ± 1.5$^+$ (n = 10)
% Fractional shortening	46.8 ± 1.7 (n = 5)	41.5 ± 1.8$^+$ (n = 8)	39.9 ± 1.4$^+$ (n = 10)
Peak E velocity (mm/s)	758 ± 24 (n = 5)	825 ± 35 (n = 6)	811 ± 22 (n = 8)
Deceleration time of the E wave (ms)	37.6 ± 1.3 (n = 5)	43.6 ± 1.5$^+$ (n = 6)	38.0 ± 1.3* (n = 8)
Peak A velocity (mm/s)	522 ± 21 (n = 5)	445 ± 34 (n = 6)	475 ± 23 (n = 8)
E/A ratio	1.46 ± 0.06 (n = 5)	1.88 ± 0.07$^+$ (n = 6)	1.73 ± 0.07$^+$ (n = 8)
Isovolumic relaxation time (ms)	22.8 ± 1.1 (n = 5)	33.3 ± 1.9$^+$ (n = 6)	27.5 ± 1.7^{+*} (n = 8)
Peak E′ velocity (mm/s)	57.0 ± 1.9 (n = 5)	37.5 ± 2.1$^+$ (n = 6)	44.9 ± 2.7^{+*} (n = 8)
Peak A′ velocity (mm/s)	55.7 ± 1.4 (n = 5)	46.7 ± 1.5$^+$ (n = 6)	47.6 ± 1.8$^+$ (n = 8)
E′/A′ ratio	1.03 ± 0.04 (n = 5)	0.80 ± 0.04$^+$ (n = 6)	0.94 ± 0.02* (n = 8)
E/E′ ratio	13.3 ± 0.3 (n = 5)	22.1 ± 0.4$^+$ (n = 6)	18.4 ± 0.4^{+*} (n = 8)

Data are the mean ± SEM. $^+P<0.05$ vs. the YC group, $^*P<0.05$ vs. the AL group.
LV mass (uncorrected) (mg) = 1.053 × [(LVIDd + LVPWd + IVSd)^3 − (LVIDd)^3].
LV, left ventricular; LVIDd; LV internal diameter (diastole) (mm), LVPWd; LV posterior wall (diastole) (mm), IVSd; interventricular septum (diastole) (mm), YC, young controls; AL, rats fed the normal control diet ad libitum; CR, rats fed a caloric-restricted diet. Because of technical difficulty, Pulse-wave Doppler evaluation was achieved in 6 AL and 8 CR rats.

3.4. Histological examination and lipofuscin content

Histological analysis revealed that long-term CR significantly reduced cardiomyocyte size (Figs. 1(A and B)) and attenuated the accumulation of lipofuscin (Figs. 1(C and D)) and senescence-associated β-galactosidase (Fig. 1(E)). Aged AL rats showed an 8-fold increase in myocardial lipofuscin content, compared with young rats, and CR attenuated this increase by 40% (Fig. 1(D)). CR also reduced TUNEL-positive cells (Figs. 2(A and B)). However, the degree in cardiac fibrosis was similar between AL and CR (Figs. 2(C–E)).

3.5. Measurement of $[Ca^{2+}]_i$

We isolated an average of 1×10^7 ventricular myocytes, 80% of which are rod-shaped, from the young heart. In contrast, fewer isolated ventricular myocytes were obtained from aged rat heart. Of these, approximately one third were rod-shaped, indicating that aging attenuates the myocyte isolation yield. However, we did not find any difference in the myocyte isolation yield between the AL and CR aged hearts.

Fig. 3(A) shows the representative Fluo-4 line scan images, their corresponding $[Ca^{2+}]_i$ transients, and the traces of myocyte contractions in isolated myocytes obtained from AL and CR rats. There were no differences in peak amplitude of $[Ca^{2+}]_i$ transients, expressed as F/F_0 (Fig. 3(B)) between the two groups. In contrast, cardiomyocytes obtained from CR rats exhibited better Ca^{2+} uptake, as evidenced by a significantly decreased time to 50% relaxation (RT_{50}; Fig. 3(C)) and the tendency for a decrease of the τ of $[Ca^{2+}]_i$ decline in cardiomyocytes

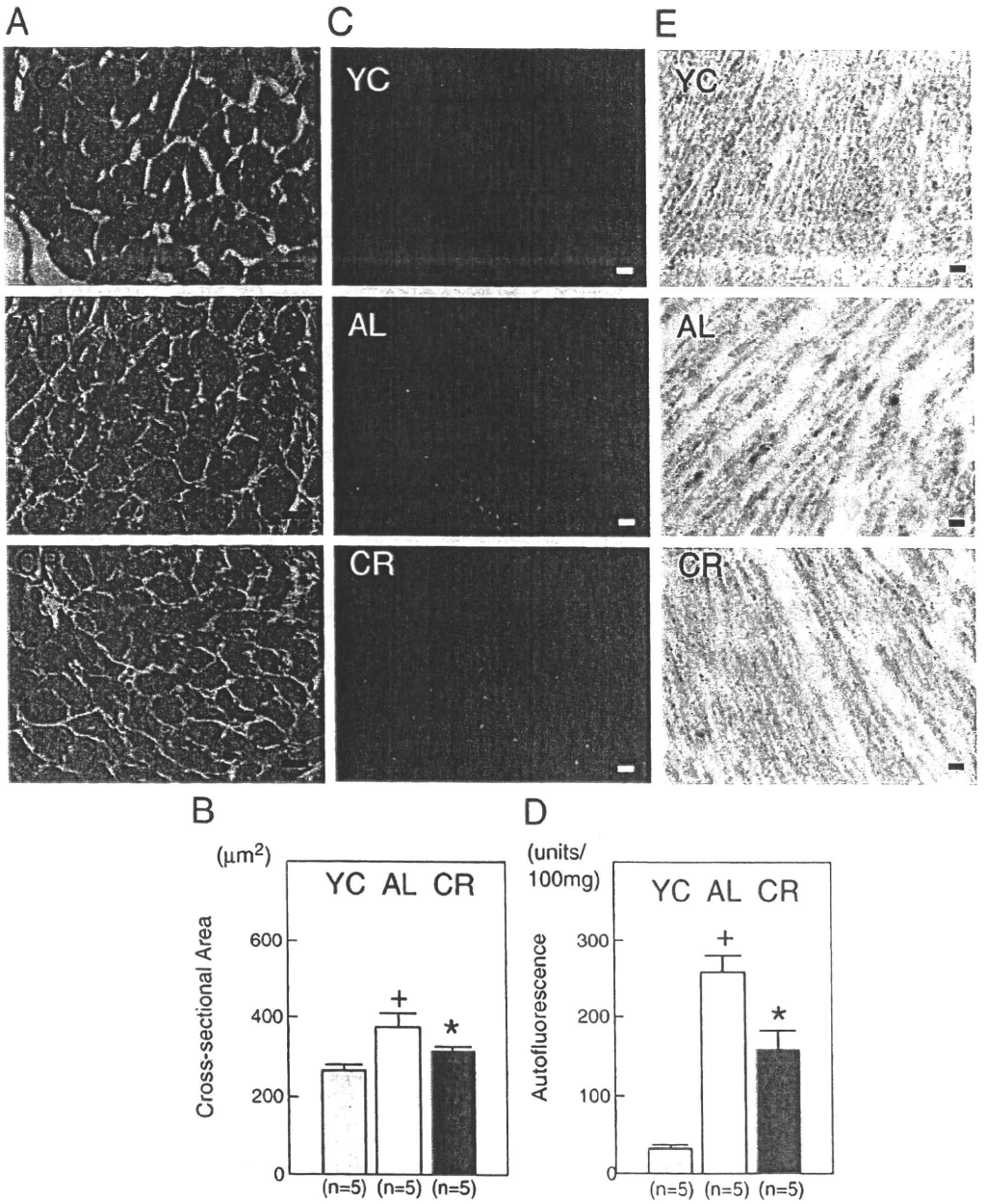

Fig. 1. Histological examination. (A) Hematoxylin and Eosin staining. (B) Cross-sectional view of cardiomyocytes in AL and CR rats. (C) Lipofuscin. (D) Myocardial lipofuscin content. (E) Senescence-associated β-galactosidase. Bar: 50 μm. YC: young controls, AL: rats fed the normal control diet ad libitum, CR: rats fed a caloric-restricted diet. Data are the mean ± SEM. Quantitative data are pooled data from 5 AL hearts and 5 CR hearts. $^{+}P<0.05$ vs. the YC group. $^{*}P<0.05$ vs. the AL group.

obtained from CR rats (Fig. 3(D)). Corresponding with these results, cardiomyocytes obtained from CR rats exhibited better relaxation, as evidenced by a decreased RT_{50} (Fig. 3(F)), although there was no difference in fractional shortening between the groups (Fig. 3(E)) These results suggested that better Ca^{2+} uptake results in better myocyte relaxation in hearts from CR rats. However, CR did not increase the SR Ca^{2+} content in the aged heart (Fig. 3(G)).

3.6. SERCA activity

SERCA activity significantly decreased with aging, but CR enhanced SERCA activity by 30% in the aged heart {YC: 205 ± 6 (n = 5), AL: 88 ± 5 (n = 3), CR: 114 ± 6 (n = 5) nmol/mg protein/min; $P<0.05$ YC vs. AL, $P<0.05$ AL vs. CR}.

3.7. Western immunoblotting

The oxyblot analysis demonstrated that protein carbonyls increased with aging and CR attenuated this increase (Fig. 4(A)), suggesting that long-term CR reduces oxidative stress in the aged heart.

Expression of senescence markers was compared among three groups. The expression of $p16^{INK4a}$ increased with aging in the AL group, and this increase was attenuated in the CR group (Figs. 4(B and C)). In contrast, CR failed to attenuate the decrease in phosphorylated troponin I at the $Ser^{23/24}$ residue (P-troponin I) with aging (Figs. 4(B and D)). It is well known that the expression of SERCA2 protein decreases with aging and this phenomenon contributes, in part, to impaired cardiac diastolic dysfunction associated with aging [5,21]. In the present study, long-term CR significantly attenuated the decrease